Preprints (www.preprints.org) | NOT PEER-REVIEWED | Posted: 17 September 2020 doi:10.20944/preprints202009.0373.v1

Article

Optimal Operation of Conventional Power Generation with High Penetration of Renewable Energy using Equilibrium Optimizer Technique

Khaled Nusair [1] **and Lina Alhmoud** [2,*]

[1] Protection and Metering Department, National Electric Power Company, Amman 11181,Jordan; khalednusair2016@yahoo.com

[2] Department of Power Engineering, Hijjawi Faculty for Engineering Technology, Yarmouk University, Irbid 21163,Jordan;lina.hmoud@yu.edu.jo

* Correspondence: lina.hmoud@yu.edu.jo

Abstract: Over the last decades, the energy market around the world has reshaped due to accommodating the high penetration of renewable energy resources. Although renewable energy sources have brought various benefits, including low operation cost of wind and solar PV power plants, and reducing the environmental risks associated with the conventional power resources, they have imposed a wide range of difficulties in power system planning and operation. Naturally, classical optimal power flow (OPF) is a nonlinear problem. Integrating renewable energy resources with conventional thermal power generators escalates the difficulty of the OPF problem due to the uncertain and intermittent nature of these resources. To address the complexity associated with the process of the integration of renewable energy resources into the classical electric power systems, two probability distribution functions (Weibull and lognormal) are used to forecast the voltaic power output of wind and solar photovoltaic, respectively. Optimal power flow, including renewable energy, is formulated as a single-objective and multi-objective problem in which many objective functions are considered, such as minimizing the fuel cost, emission, real power loss, and voltage deviation. Real power generation, bus voltage, load tap changers ratios, and shunt compensators values are optimized under various power systems' constraints. This paper aims to solve the OPF problem and examines the effect of renewable energy resources on the above-mentioned objective functions. A combined model of wind integrated IEEE 30-bus system, solar PV integrated IEEE 30-bus system, and hybrid wind and solar PV integrated IEEE 30-bus system are performed using the equilibrium optimizer technique (EO) and other five heuristic search methods. A comparison of simulation and statistical results of EO with other optimization techniques showed that EO is more effective and superior.

Keywords: Active power loss; total generation cost; emission index; optimal power flow; equilibrium optimizer; solar PV integrated IEEE 30-bus system; wind integrated IEEE 30-bus system; hybrid wind and solar PV integrated IEEE 30-bus system

1. Introduction

1.1. Background

The urgent need for reducing the fuel cost of the conventional power generation units and minimizing the greenhouse gases emitted from the thermal power generators have led various electric power companies to go toward utilizing renewable energy resources. Furthermore, advanced technologies of renewable energy resources have contributed significantly to be the most inexpensive and environmentally friendly. Integrating wind and solar PV in proper locations and appropriate settings of the variables of the conventional power networks may have a significant impact on the performance of power system control and operation.

© 2020 by the author(s). Distributed under a Creative Commons CC BY license.

Preprints (www.preprints.org) | NOT PEER-REVIEWED | Posted: 17 September 2020 doi:10.20944/preprints202009.0373.v1

To make the modeling of wind and solar PV more accurate and realistic, the Weibull probability distribution function was used to forecast the wind speed [1]-[2]. Whereas lognormal probability distribution function is used to mimic the intermittent nature of solar irradiance in [3] [4].

1.2. Literature review

Numerous publications in the literature studied the optimal power flow (OPF) problem for systems consisting of conventional power generation and renewable-energy power plants. Deterministic, stochastic or hybrid optimization methods are used extensively to address the issues associated with increased penetration of non-dispatchable renewable energy, advanced controls such as FACTs devices and deregulated electricity markets.

Various conventional optimization techniques are used to solve the OPF problem. For instance, continuous nonlinear programming was proposed [5]. An extended conic quadratic format [6] is presented to solve the economic dispatch and decrease real power loss. Besides, the predictor-corrector interior point algorithm is proposed to fit the OPF for solving nonlinear programming problems [7]. Quadratic programming is used to derive a loss formula based on the incremental power flow [8]. Sequential quadratic programming is used to address large scale OPF; it also depends on transforming the original problem to a sequence of linearly constrained sub-problem by applying an augmented lagrangian [9]. Mixed-integer linear programming to minimize transmission losses and reactive generator outputs are adapted [10]. Although these methods have excellent convergence characteristics, they have various drawbacks, including failing to find the global solution because of non-convexity and facing difficulty while handling the problems with non-differentiable and discontinuous objective functions.

Recently, metaheuristic optimization algorithms have been gaining much attention due to flexibility, free of derivation, and local optima avoidance. Thus, single and multi-objective optimization methods overcome the shortcomings attributed to classical techniques. A gravitational search algorithm to find the optimal solution for OPF and IEEE 30-bus and 57-bus systems are examined [11]. The basic fuel cost, voltage profile, voltage stability, and non-smooth quadratic cost are minimized and optimized using a differential evolution algorithm [12]. The Black hole-based optimization method is used to address the OPF problem for IEEE 30-bus and Algerian 59-bus power systems [13]. Constrained OPF problem for IEEE 30-bus, 57-bus, and 118-bus is optimized using a moth swarm algorithm [14]. A multi-objective OPF to minimize the generation cost and environmental pollution using a fuzzy membership function to choose a compromise solution from the Pareto optimal solutions is discussed [15]. The fuel cost, voltage deviation, and real power loss are minimized as a multi-objective OPF problem using a gravitational search algorithm [16]. A modified teaching learning-based optimization algorithm added a self-adapting wavelet mutation strategy and a fuzzy clustering [17]. A hybrid of fuzzy evolutionary and swarm optimization is proposed to minimize the cost of active power generation and real power losses [18].

A fuzzy-based modified bee colony is presented to solve discrete OPF using multi-objective mixed integer nonlinear [19]. Emission, real power losses, and voltage deviation are all minimized as a multi-objective OPF using a multi-objective modified imperialist competitive algorithm [20]. The particle swarm optimization and the shuffled frog leaping algorithm are hybridized to solve OPF using the generator's constraints such as prohibited zones and valve point effect [21]. A chaotic invasive weed optimization algorithm is proposed to solve the OPF problem with non-smooth and non-convex fuel cost curves [22]. Brainstorming optimization and teaching-learning optimization are hybridized to minimize the fuel cost of thermal generation units [23]. A hybrid optimization algorithm is based on sequential quadratic programming to generate an initial population. Then a differential evolution took that population to find the optimal solution more effectively and it was used to minimize the fuel cost with valve point and the transmission line real losses [24].

A growing and considerable effort have been made in recent years to solve and model the OPF problem, including renewable energy sources. The OPF problem with taking into account uncertainties in the wind, solar, and load forecast and optimized using a genetic algorithm and two-point estimate method [25]. A hybrid method called moth swarm algorithm and gravitational search algorithm is used to solve the problem of OPF, including wind power [26]. A modified two-point estimation method is used to solve probabilistic OPF incorporating wind and solar photovoltaic [27]. Hybrid wind photovoltaic power systems are optimized using the unscented transformation method, which can carry out probabilistic OPF with high accuracy and less computational time

Preprints (www.preprints.org) | NOT PEER-REVIEWED | Posted: 17 September 2020 doi:10.20944/preprints202009.0373.v1

[28]. The OPF, including wind is optimized using a fuzzy-based particle swarm optimization. A fuzzy set modeled the forecast load demand and wind speed [29].

Besides, OPF incorporating wind power energy is optimized by a hybrid algorithm called a hybrid dragonfly with aging particle swarm optimization [30]. Adaptive differential evolution with proper constraint handling method is addressed OPF, including wind and solar. The forecast wind and solar photovoltaic are modeled using Weibull and lognormal probability distribution functions [31]. An optimal reactive power dispatch with solar photovoltaic power and its impact on minimizing real power losses is addressed using the Jaya algorithm to solve this issue [32]. A constrained multi-objective population external optimization method in [33] is presented to minimize the fuel cost and emission in the presence of renewable energy sources. A grey wolf optimization algorithm in [34] was proposed to tune the parameters of a thyristor controlled series compensator and address OPF, including wind and solar power. A gbest guided artificial bee colony optimization in [1] was to find the optimal setting of conventional and renewable power generation.

1.3. Contribution and paper organization

In the present work, an equilibrium optimizer [35], which is a novel optimization method inspired by controlling the volume mass balance model for estimating both equilibrium and dynamic states, is used to prove its performance in solving the OPF problem. It is implemented on i) IEEE 30-bus system, ii) wind integrated IEEE 30-bus system, iii) solar PV integrated IEEE 30-bus system, and iv) hybrid wind and solar PV integrated IEEE 30-bus system. Real power loss minimizations, total cost minimization of generating units and emission index minimization are considered to be the objective functions of the OPF problem. Weibull and lognormal probability distribution functions are used to model the wind speed and solar irradiance to forecast the output power of wind and solar PV systems. Furthermore, aiming to fill the gap in the literature, this paper investigates the impact of the presence of only wind or only solar PV or both of them on enhancing the objective functions of the OPF problem. In addition, a comprehensive statistical analysis for the equilibrium optimizer technique (EO) and other optimization techniques are analysed.

The rest of this paper is organized as follows: the formulation of OPF problem is described in Section 2. Then, a mathematical models of wind and solar PV plants are introduced in Section 3. Section 4 presents the equilibrium optimizer technique (EO) and its implementation to solve the OPF problem. Simulation results are explained in Section 6. Finally, Section 7 draws the conclusion of this work.

2. Problem formulation of OPF

2.1. General structure of OPF

Generally, OPF aims to minimizes some objective functions. f_o is the objective function to be minimized ,and h and g are the equality and inequality constraints in the power system network, OPF can be expressed as [14,36] :

$$\begin{array}{ll} \text{Minimize} & f_o(x,u) \\ \text{Subject to} & g(x,u) \leq 0 \\ & h(x,u) = 0 \end{array} \tag{1}$$

x is a state vector of dependent variables including real power of swing generator (P_{G_1}), (V_{L_i}) is the voltage magnitude of load buses, (Q_{G_i}) is the reactive power of generator at i_{th} bus and (S_{l_i}) is the loading of the i_{th} transmission line. x can be expressed as follows [14,36]:

$$x = [P_{G_1}, V_{L_1}, \ldots, V_{L_{npq}}, Q_{G1}, \ldots, Q_{G_{NG}}, S_{l_1}, \ldots, S_{l_{n_l}}]^T \tag{2}$$

where npq, and n_l are the number of PQ buses and transmission lines. S_l and n_l are loading of transmission lines and the number of transmission lines, respectively.

Preprints (www.preprints.org) | NOT PEER-REVIEWED | Posted: 17 September 2020 doi:10.20944/preprints202009.0373.v1

u is a vector consisting of control variables, (P_{G_i}) is the real power of all generators excluding swing generator, (V_{G_i}) is the voltage magnitude of generators, (TS) is the branch transformer tap, and (Q_C) is the shunt capacitors. u can be expressed as follows [14,36]:

$$u = [P_{G_2}, \ldots, P_{G_{NG}}, V_{G_1}, \ldots, V_{G_{NG}}, Q_{C1}, \ldots, Q_{CN_c}, TS_1, \ldots, TS_{N_T}]^T \tag{3}$$

where, NG, N_c and N_T are the number of generators, shunt VAR compensator and transformers, respectively.

2.2. Objective functions of OPF

Here, the first four cases dealt with solving single objective OPF and the last one addressed the multi-objective OPF.

- Case 1: real power loss minimization
  Due to the presence of the inherent resistance for the transmission lines, the aim of this function is to minimize the active power losses and it is expressed as [14,36]:

$$f_o(x,u) = P_{loss} = \sum_{q=1}^{nl} G_{q_{(ij)}} (V_i^2 + V_j^2 - 2V_iV_j \cos\ (\delta_{ij})) \tag{4}$$

  Where $G_{q(ij)}$ is the conductance of q_{th} transmission line, and V_i and V_j are the voltage magnitude of terminal buses of transmission line.
- Case 2: emission index minimization
  In the present case, the target is to reduce the harmful gases emission from the thermal generation units, and the coefficients of the gas emission of the thermal power generators are given in Table 1. Emission in tons per hour (t/h) can be described by [14,36]:

$$f_o(x,u) = E = \sum_{i=1}^{NG} [(\alpha_i + \beta_i P_{G_i} + \gamma_i P_{G_i}^2) * 0.01 + \omega_i e^{(\mu_i P_{G_i})}] \tag{5}$$

  where α, β, γ, ω and μ are the emission coefficient and they are given in Table 1.

Table 1. Emission coefficients of thermal power generating units.

Generator	Bus	α	β	γ	ω	μ
G1	1	4.091	-5.554	6.49	0.0002	2.857
G2	2	2.543	-6.047	5.638	0.0005	3.333
G3	5	4.258	-5.094	4.586	0.000001	8
G4	8	5.326	-3.55	3.38	0.002	2
G5	11	4.258	-5.094	4.586	0.000001	8
G6	13	6.131	-5.555	5.151	0.00001	6.667

- Case 3: Basic fuel cost minimization
  The relationship between fuel cost ($\$/h$) and the power generated from the thermal generating units can be approximately given by the quadratic relationship and it is expressed as [14,36]:

$$f_o(x,u) = FC = \sum_{i=1}^{NG} a_i + b_i P_{G_i} + c_i P_{G_i}^2 \tag{6}$$

  where a_i, b_i, c_i are the cost coefficient of the thermal generators and these coefficients are provided in Table 2.

Preprints (www.preprints.org) | NOT PEER-REVIEWED | Posted: 17 September 2020 doi:10.20944/preprints202009.0373.v1

Table 2. Cost coefficients of the thermal power generators.

Generator	Bus	a	b	c
G1	1	0	2	0.00375
G2	2	0	1.75	0.0175
G3	5	0	1	0.0625
G4	8	0	3.25	0.00834
G5	11	0	3	0.025
G6	13	0	3	0.025

- Case 4: Voltage deviation minimization
  The voltage deviation index is the cumulative deviation of all load buses from nominal value of unity. It also play a significant role in keeping the voltage quality and security of the electrical power network.This case is expressed as [14,36]:

$$f_o(x,u) = VD = \left(\sum_{p=1}^{NL} |V_{L_p} - 1| \right) \tag{7}$$

- Case 5: Minimization of basic the fuel cost, emission index,voltage deviation and the real power losses.
  The aim of this case is to reduce quadratic fuel cost, active power transmission losses, environmental emission index and voltage deviation index simultaneously. It can be defined as follows[14,36]:

$$f_o(x,u) = \sum_{i=1}^{NG} a_i + b_i P_{G_i} + c_i P_{G_i}^2 + \lambda_p \times P_{loss} + \lambda_{VD} \times VD + \lambda_E \times E \tag{8}$$

where λ_p, λ_{VD} and λ_E are weight factors and they are assumed to be 22, 21 and 19, respectively as in [14].

2.3. Constraints

The constraints of OPF are usually categorized into [14,36]:

1. Equality constraints
   The equality constraints of OPF are usually represented by the load flow equations:

$$P_{G_i} - P_{D_i} = V_i \sum_{k=1}^{N_B} V_k (G_{ik} \cos\ \theta_{ik} + B_{ik} \sin\ \theta_{ik}) \tag{9}$$

$$Q_{G_i} - Q_{D_i} = V_i \sum_{k=1}^{N_B} V_k (G_{ik} \sin\ \theta_{ik} - B_{ik} \cos\ \theta_{ik}) \tag{10}$$

   where P_{D_i}, Q_{D_i}, N_B,and θ_{ik} are the active and reactive load demand,the reactive load demand , the number of buses and the angle difference between bus i and k ,respectively. G_{ik} and B_{ik} are the transfer and susceptance conductance.
2. Inequality constraints
   It can be defined by operating limits on the equipment of the power system, transmission loading and voltage of load buses.

   (a) Constraints of thermal and renewable energy generating units

$$V_{G_{i,min}} \leq V_{G_i} \leq V_{G_{i,max}} i = 1,\ldots,N \tag{11}$$

$$P_{G_{i,min}} \leq P_{G_i} \leq P_{G_{i,max}} i = 1,\ldots,N \tag{12}$$

$$Q_{G_{i,min}} \leq Q_{G_i} \leq Q_{G_{i,max}} i = 1,\ldots,N \tag{13}$$

   (b) Constraints of the transformer tap setting

$$TS_{k,min} \leq TS_k \leq TS_{k,max} k = 1,\ldots,N_T \tag{14}$$

Preprints (www.preprints.org) | NOT PEER-REVIEWED | Posted: 17 September 2020 doi:10.20944/preprints202009.0373.v1

(c) constraints of the shunt compensator

$$Q_{C,j,min} \leq Q_C \leq Q_{C,j,max} j = 1,\ldots,N_C \tag{15}$$

(d) Constraints of the voltages at load buses

$$V_{Lr,min} \leq V_{Lr} \leq V_{Lr,max} r = 1,\ldots,N_L \tag{16}$$

(e) Constraints of the transmission line loading

$$S_{lv} \leq S_{lv,max} v = 1,\ldots,n_l \tag{17}$$

2.4. Constraint handling

In order to decline the infeasible solutions of OPF and keep the dependent variables within the allowable ranges , a penalty function was modeled and added to the objective functions defined in Section 2.2 [14,36].

$$penalty = K_p(P_{G1} - P_{G1}^{Lim})^2 + K_Q \sum_{i=1}^{NG}(Q_{Gi} - Q_{Gi}^{Lim})^2 + K_V \sum_{i=1}^{NL}(V_{Li} - V_{Li}^{Lim})^2 + K_S \sum_{i=1}^{nl}(S_{li} - S_{Li}^{Lim})^2 \tag{18}$$

where K_Q, K_p, K_V and K_S are the values of penalty factors associated with generation reactive power, generation real power of the swing generator, load bus voltages and line flow of transmission lines . They are assumed to be 100, 100, 100, and 100,000, respectively [14,37], and x^{Lim} is the value of the violated limit of dependent variables(x). It is equal to x^{max} in case of $x > x^{max}$ or x^{min} in case of $x < x^{min}$.

3. Mathematical models of the wind & solar power generating units

3.1. Wind power units

3.1.1. Uncertain and power model of wind turbines

The wind speed of the wind turbines follows the Weibull probability distribution function. The characteristic of the output power generated by the wind turbine is a random variable depending on wind speed. The Weibull probability distribution function with dimensionless shape factor (k) and scale factor (c) is used to model the wind speed $f_{(v)}(v)$. The wind speed ($f_{(v)}(v)$) can be expressed mathematically as [1,2,38,39]:

$$f_v(v) = \frac{k}{c}\left(\frac{v}{c}\right)^{k-1} \times e^{-\left(\frac{v}{c}\right)^k} \tag{19}$$

Mean of Weibull distribution (M_{wbl}) can be expressed as [31,40–42]:

$$M_{wbl} = c * \Gamma(1 + K^{-1}) \tag{20}$$

The electrical energy generated by a wind turbine $(P_w(v))$ is the result of converting of the kinetic energy of wind and it can be estimated as [1,2,38,39]:

$$P_w(v) = \begin{cases} 0 & v < v_{in} \text{ and } v > v_{out} \\ P_{wr}\left(\dfrac{v - v_{in}}{v_r - v_{in}}\right) & v_{in} \leq v \leq v_r \\ P_{wr} & v_r < v \leq v_{out} \end{cases} \tag{21}$$

where (P_{wt}), (v_{in}), (v_{out}) and (v_r) are the rated power of the wind turbine, the cut-in wind speed of the wind turbine, the cut-out wind speed and the rated wind speed, respectively.

Preprints (www.preprints.org) | NOT PEER-REVIEWED | Posted: 17 September 2020 doi:10.20944/preprints202009.0373.v1

140 3.1.2. Calculation of direct, underestimation and overestimation cost of wind power

The direct cost of wind power plant can be defined as[31,40–42]:

$$C_{w,j}(P_{ws,j}) = g_j P_{ws,j} \tag{22}$$

where g_j is the direct cost coefficient of wind plant. The cost function is overestimated because the actual generated power from the wind turbine is less than the estimated power by mathematical equations. The overestimation cost is used for reverse the requirements when the estimated output power of the wind turbine is more than actual output power. Reserve cost for the j^{th} wind turbine can be defined as [31,40–42]:

$$\begin{aligned} C_{Rw,j}(P_{ws,j} - P_{wav,j}) &= K_{Rw,j}(P_{ws,j} - P_{wav,j}) \\ &= K_{Rw,j} \int_0^{P_{ws,j}} (P_{ws,j} - P_{w,j}) f_w(P_{w,j}) dP_{w,j} \end{aligned} \tag{23}$$

where $K_{Rw,j}$, $P_{wav,j}$, $P_{ws,j}$ and $f_{w(pw,j)}$ are the reserve cost coefficient pertaining to j^{th} wind turbine, the actual available power from the same plant, the estimated power from the j^{th} wind turbine and the wind power probability density function for j^{th} wind turbine. Underestimation cost function of the wind turbine is due to not using the whole power which is generated from the wind turbine. In other words, when the generated power from the wind turbine is more than the estimated power, underestimation cost function is applied as a penalty due to waste the surplus power. The Penalty cost for the j^{th} wind turbine can be defined as [31,40–42]:

$$\begin{aligned} C_{Pw,j}(P_{wav,j} - P_{ws,j}) &= K_{Pw,j}(P_{wav,j} - P_{ws,j}) \\ &= K_{Pw,d} \int_{P_{ws,j}}^{P_{wr,j}} (P_{w,j} - P_{ws,j}) f_w(P_{w,j}) dP_{w,j} \end{aligned} \tag{24}$$

where $K_{Pw,j}$ is a coefficient represent the penalty cost for the j^{th} wind turbine and $P_{wr,j}$ is the rated output power which is generated from the j^{th} wind turbine. As shown in Section 3.1.2, the total cost of wind power turbines (C_T^W) can be described as follows:

$$C_T^W = \sum_{j=1}^{N_w} C_{w,j}(P_{ws,j}) + C_{Rw,j}(P_{ws,j} - P_{wav,j}) + C_{Pw,j}(P_{wav,j} - P_{ws,j}) \tag{25}$$

141 where N_w is the number of wind power turbines.

142 *3.2. Solar power units*

143 3.2.1. Uncertain and power model of solar PV plants

Solar irradiance can be modelled by Lognormal probability distribution function due to its uncertain and stochastic nature. The Lognormal probability distribution is a function of solar irradiance (G) with mean μ and standard deviation σ , it can be expressed mathematically as [3],and [4]:

$$f_G(G) = \frac{1}{G\sigma\sqrt{2\pi}} \exp\left(\frac{-(lnx - \mu)^2}{2\sigma^2}\right) G > 0 \tag{26}$$

Mean of lognormal distribution M_{lgn} can be expressed as:

$$M_{lgn} = \exp\left(\mu + \frac{\sigma^2}{2}\right) \tag{27}$$

Preprints (www.preprints.org) | NOT PEER-REVIEWED | Posted: 17 September 2020 doi:10.20944/preprints202009.0373.v1

The main role of PV systems is to convert the solar irradiance to electrical energy. The output power of PV system $(P_s(G))$ as a function of irradiance can be estimated as [31,40]:

$$P_s(G) = \begin{cases} P_{sr}\dfrac{G^2}{G_{std}R_c} & \text{for } 0 < G < R_c \\ P_{sr}\dfrac{G}{G_{std}} & \text{for } G \geq R_c \end{cases} \tag{28}$$

where G_{std} represents the solar irradiance in standard environment,R_c is a certain irradiance point ,and P_{sr} is the rated output power which is generated from the solar PV system.

3.2.2. Calculation of direct,underestimation,and overestimation cost of solar PV power

The direct cost of solar power plant can be defined as [31,40] :

$$C_{s,k}(P_{ss,k}) = h_k P_{ss,k} \tag{29}$$

where h_k is a coefficient represents the direct cost of solar photovoltaic plant.
The same case as in wind energy system, solar energy system in involves overestimation and underestimation cost due its uncertain output power. Reserve cost for the overestimation ofk^{th} solar PV system is [31,40]:

$$\begin{aligned} C_{Rs,k}(P_{ss,k} - P_{sav,k}) &= K_{Rs,k}(P_{ss,k} - P_{sav,k}) \\ &= K_{Rs,k} * f_s(P_{sav,k} < P_{ss,k}) * \\ &\quad [P_{ss,k} - E(P_{sav,k} < P_{ss,k})] \end{aligned} \tag{30}$$

where $K_{Rs,k}$ is a coefficient represents the reserve cost pertaining to k^{th} solar PV system, $P_{sav,k}$ is the actual available power from the same plant, $f_s(P_{sav}, k < P_{ss,k})$ is the probability of solar power shortage occurrence than the scheduled power $(P_{ss,k})$ and $E(P_{sav,k} < P_{ss,k})$ is the expectation of solar PV power below $P_{ss,k}$.
In case of the underestimation of k^{th} solar PV system, the penalty cost is given as [31,40]:

$$\begin{aligned} C_{Ps,k}(P_{sav,k} - P_{ss,k}) &= K_{Ps,k}(P_{sav,k} - P_{ss,k}) \\ &= K_{Ps,k} * f_s(P_{sav,k} > P_{ss,k}) * \\ &\quad [E(P_{sav,k} > P_{ss,k}) - P_{ss,k}] \end{aligned} \tag{31}$$

where $K_{Ps,k}$ is a coefficient represents the penalty cost pertaining to k^{th} solar PV system, $f_s(P_{sav,k} < P_{ss,k})$ is the probability of solar power surplus than the scheduled power $(P_{ss,k})$ and $E(P_{sav,k} < P_{ss,k})$ is the expectation of solar PV power above $P_{ss,k}$. As explained in Section 3.2.2, the total cost of solar PV plants (C_T^{PV}) consists of three terms(direct, underestimation and overestimation cost) and it can be given as follow [31,40]:

$$C_T^{PV} = \sum_{k=1}^{N_{PV}} C_{s,k}(P_{ss,k}) + C_{Ps,k}(P_{sav,k} - P_{ss,k}) + C_{Rs,k}(P_{ss,k} - P_{sav,k}) \tag{32}$$

where N_{PV} is the number of the solar PV plants.

4. Proposed EO

4.1. Inspiration and mathematical model

The main inspiration for this algorithm is the dynamic mass balance equation which describes the conservation of mass which enters, leaves or generates in a control volume. This equation is a first-order ordinary differential equation and it is described as following [35]:

$$V\frac{dC}{dt} = QC_{eq} - QC + G \tag{33}$$

Preprints (www.preprints.org) | NOT PEER-REVIEWED | Posted: 17 September 2020 doi:10.20944/preprints202009.0373.v1

where $V\frac{dC}{dt}$ is the rate of change of mass in volume, (V),C is the concentration inside the volume(V), V is the control volume, Q is the volumetric flow rate into and out of the control volume, C_{eq} is the concentration at an equilibrium state.

After reaching the steady equilibrium state of equation (33) that is reformulated as a function of $\left(\frac{Q}{V}\right)$ which is called turnover rate $\left(\lambda = \frac{Q}{V}\right)$. The following equations are derived from equation (33) to solve for (C) as a function of time (t) [35]:

$$\frac{dC}{\lambda C_{eq} - \lambda C + \frac{G}{V}} = dt \tag{34}$$

$$\int_{C_0}^{C} \frac{dC}{\lambda C_{eq} - \lambda C + \frac{G}{V}} = \int_{t_0}^{t} dt \tag{35}$$

$$F = e^{-\lambda(t-t_0)} \tag{36}$$

$$C = C_{eq} + (C_0 - C_{eq})F + \frac{G}{\lambda V}(1-F) \tag{37}$$

where F ,t_0 is the initial start time and C_0 is the initial concentration.

The equation (37) introduces three rules for updating the concentration of each particle. The equilibrium concentration is the first term which is described as one of the best-so-far solutions randomly chosen from the equilibrium pool. The difference between a concentration of a particle and the equilibrium state is the second term which helps particles to globally explore the domain. The final term is called the generation rate which mainly acts as an exploiter or solution refiner [35].

4.2. The interaction between each term and the search pattern and the definition of the EO's terms

4.2.1. Initialization and function evaluation

Firstly, the optimization process starts with the initial population. The equation (38) describes the initial concentration process which depends on the number of particles and dimensions that initialized in the search space in a uniform random manner [35].

$$C_i^{initial} = C_{min} + rand_i\,(C_{max} - C_{min}) \tag{38}$$

where $C_i^{initial}$ is the initial concentration vector of the ith particle, C_{min} is the minimum value for the dimensions, C_{max} is the maximum value for the dimensions and $rand_i$ is a random vector ranges between zero and one. After that, the fitness function of the particles are evaluated and then solved to determine the equilibrium conditions.

4.2.2. Equilibrium pool and candidates (C_{eq})

The global optimum of EO is represented by the equilibrium state. At the beginning, no information about the equilibrium state is existed, but equilibrium candidates are identified to provide a search domain for the particles. There are five equilibrium candidates as given in equation 39. Four of them are the best-so-far particles determined during the optimization process and the last one is the arithmetic mean of the previous-mentioned four particles. The main goal of the first four candidates is to improve the exploration capability, whereas the fifth candidate enhances the exploitation [35]

$$C_{avg} = \overrightarrow{C}_{eq}(1) + \overrightarrow{C}_{eq}(2) + \overrightarrow{C}_{eq}(3) + \overrightarrow{C}_{eq}(4) \tag{39}$$

$$C_{eq,pool} = \left\{\overrightarrow{C}_{eq}(1), \overrightarrow{C}_{eq}(2), \overrightarrow{C}_{eq}(3), \overrightarrow{C}_{eq}(4), \overrightarrow{C}_{eq}(ave)\right\} \tag{40}$$

Preprints (www.preprints.org) | NOT PEER-REVIEWED | Posted: 17 September 2020 doi:10.20944/preprints202009.0373.v1

4.2.3. Exponential term (F)

The exponential term (F) helps EO to have an acceptable balance between exploration and exploitation. Referring back to equation (36), the time (t) in equation (36) depends on the iteration $(Iter)$ and it is described as follows [35] :

$$t = \left(1 - \frac{Iter}{Max_{iter}}\right)^{\left(a_2 \frac{Iter}{Max_{iter}}\right)} \tag{41}$$

For the purpose of convergence, t_0 in equation (10) is proposed to slow down the search speed as well as enhancing the exploration and exploitation ability of EO [35].

$$t_0 = \frac{1}{\overrightarrow{\lambda}} ln\left(-a_1 sign(\overrightarrow{r} - 0.5)[1 - e^{-\overrightarrow{\lambda} t}]\right) \tag{42}$$

where a_1 and a_2 are constant values for controlling exploration and exploitation ability, $sign(\overrightarrow{r} - 0.5)$ is a factor that determine the direction of exploration and exploitation and r is a random vector ranges between zero and one.

4.2.4. The generation rate (G)

The generation rate aims to provide the exact solution by enhancing the exploitation ability of EO and can be described as [35]:

$$\overrightarrow{G} = \overrightarrow{G_0} e^{-\overrightarrow{k}(t - t_0)} \tag{43}$$

After assumption that $k = \lambda$,the equation of generation rate was updated as follows [35]:

$$\overrightarrow{G} = \overrightarrow{G_0}\overrightarrow{F} \tag{44}$$

$$\overrightarrow{G_0} = \overrightarrow{GCP}\left(\overrightarrow{C_{eq}} - \overrightarrow{\lambda}\overrightarrow{C}\right) \tag{45}$$

$$\overrightarrow{GCP} = \begin{cases} 0.5r_1, & r_2 \geq GP \\ 0, & r_2 \geq GP \end{cases} \tag{46}$$

where r_1 and r_2 are random number between zero and one, GCP is the generation rate control parameter.
The generation rate control parameter (GCP) mainly depends on generation probability (GP) which defines the number of particles which uses generation term to update their states.
State of the art state that EO at $GP = 0.5$, EO can achieve a good balance between exploration and exploitation.
The updating rule of EO is given as:

$$\overrightarrow{C} = \overrightarrow{C_{eq}} + \left(\overrightarrow{C} - \overrightarrow{C_{eq}}\right)\overrightarrow{F} + \frac{\overrightarrow{G}}{\overrightarrow{\lambda} V}\left(1 - \overrightarrow{F}\right) \tag{47}$$

The second and third terms of equation (47) can increase variation and thus helps EO to better explore in case of they have same signs or to decrease the variation and aiding EO in local searches in case of having opposite signs [35].

4.2.5. Particle's memory saving

This can help each particle track with its coordinates in the space. It aids EO in exploitation capability and avoids getting trapped in local minima [35].

5. Implementation of EO to solve the OPF problem

The proposed EO is applied to solve OPF problem including wind and solar PV generation units. The following pseudo code explains the steps of the application of EO for OPF problem.

Preprints (www.preprints.org) | NOT PEER-REVIEWED | Posted: 17 September 2020 doi:10.20944/preprints202009.0373.v1

1. Define the control and dependent variables and their limits as well as the target objective function defined in Section 2.2.
2. Collect and read the input data of the power system under test such as data of transmission lines, transformers, shunt VAR compensator, loads and generation units.
3. Calculate the estimated output power of solar PV and wind power generation units as defined and explained in Section 3.
4. Initialize the particle's populations.
5. Assign a large number to the fitness of equilibrium candidates and let a1=2; a2=1; GP=0.5.
6. Do the main while loop as following [35]:

   (a) While (current iteration (Iter) <maximum number of iteration (Max-iter))
   (b) For i=1: particles' number (n)
   (c) Find the fitness value of the i_{th} particle

      i. If fitness (C_i) <fitness (C_{eq1}) then
      Substitute (C_{eq1}) with (C_i) and fitness (C_{eq1})
      with fitness (C_i)

      ii. Else if fitness (C_i) >fitness (C_{eq1}) & fitness (C_i) <fitness (C_{eq2}) then
      Substitute (C_{eq2}) with (C_i) and fitness (C_{eq1})
      with fitness (C_i)

      iii. Else if fitness (C_i) >fitness (C_{eq1}) & fitness (C_i)
      >fitness (C_{eq2}) & fitness (C_i) <fitness (C_{eq3}) then
      Substitute (C_{eq3}) with (C_i) and fitness (C_{eq3})
      with fitness (C_i)

      iv. Else if fitness (C_i) >fitness (C_{eq1}) & fitness (C_i) >fitness (C_{eq2}) & fitness (C_i) >fitness (C_{eq3}) & fitness (C_i) <fitness (C_{eq4}) then
      Substitute (C_{eq4}) with (C_i) and fitness (C_{eq4}) with fitness (C_i)

   (d) End (if)
   (e) End(for)

7. Find the $\overrightarrow{C_{avg}}$ according to equation (39).
8. Construct the equilibrium pool according to equation (40) [35].
9. In case of the current iteration >1, accomplish memory saving [35].
10. Assign t according to equation (41).
11. Do the second for loop as following:
    For i=1: particles' number

    (a) Select one candidate from the equilibrium pool randomly.
    (b) Create the two random vector (λ and r).
    (c) Construct F, GCP, G_0 and G according to the equation (36), equation (46), equation (45) and equation (44), respectively [35].
    (d) Update the concentration C according to equation (47)/

    End the second for loop.
12. Increase the current iteration by one.
13. End the main while loop.
14. Extract and analysis of the results.

6. Results and Discussion

The performance and effectiveness of the EO is verified for solving OPF problem by carrying out 20 independent test trial runs for all cases discussed in Section 2.2. The EO [35] and other five metaheuristic optimization techniques: MFO [43], TACPSO [44], AGPSO1 [44], TLBO [45] and MPSO [44] have been tested on four power test systems given in Section 6.1 . All these optimization techniques are implemented on 2.8-GHz i7 PC with 16 GB of RAM using MATLAB 2017.

Preprints (www.preprints.org) | NOT PEER-REVIEWED | Posted: 17 September 2020 doi:10.20944/preprints202009.0373.v1

The number of iteration, population size ,testing ranges and other parameters of the optimization methods are given in Table 3.

Table 3. Control parameters values for optimization methods.

Algorithm	Parameters	Values
MPSO [44]	Inertia coefficient (w)	decreasing linearly from 0.9 to 0.4
	Number of search agents	50
	Maximum number of iteration	100
	Udapting factor (C1,C2)	Descriped in [44]
	Acceleration coefficient (c1,c2)	c1=1, c2=2
TLBO [45]	Teaching factor	Selected randomly [1,2]
	Population size	50
	Maximum number of iteration	100
TACPSO [44]	Inertia coefficient (w)	decreasing linearly from 0.9 to 0.4
	Number of search agents	50
	Maximum number of iteration	100
	Udapting factor (C1,C2)	Descriped in [44]
	Acceleration coefficient (c1,c2)	c1=1, c2=2
MFO [43]	Population size	50
	Maximum number of iteration	100
	Shape constant (b)	1
AGPSO 1 [44]	Inertia coefficient (w)	decreasing linearly from 0.9 to 0.4
	Number of search agents	50
	Maximum number of iteration	100
	Udapting factor (C1,C2)	Descriped in [44]
	Acceleration coefficient (c1,c2)	c1=1, c2=2
EO [35]	Constant values for controlling exploration (a_1)	2
	Constant values for controlling exploitation (a_2)	1
	Number of search particles	50
	Maximum number of iteration	100
	Generation probability	0.5

6.1. Description of the test power systems

- Test system 1: IEEE 30-bus system
  The IEEE 30-bus system consists of six thermal power generators, as presented in Figure 1.The data about transmission lines, tap changing transformers, AVR compensators, limitations on generators and load voltages, active and reactive power demand are given in [46–48]. The general specifications of this system are described in Table 4.

Table 4. The general specification of all test power systems.

	Values and Details			
Characteristics	**Test system 1 [46–48]**	**Test system 2**	**Test system 3**	**Test system 4**
Buses	30	30	30	30
Transmission Lines	41	41	41	41
Limitation on generator voltage	[0.9-1.1]	[0.9-1.1]	[0.9-1.1]	[0.9-1.1]
Limitation on load voltage	[0.95-1.1]	[0.95-1.1]	[0.95-1.1]	[0.95-1.1]
Thermal power generators	6	3	3	3
Wind power plants	0	5	0	2
Solar power plants	0	0	5	3
Shunt VAR compensation	9	9	9	9
Transformer with tap ratio	4	4	4	4
Control Variables	24	28	28	28
Active and Reactive power demand	283.4 MW ,126.2 Mvar	283.4 MW ,126.2 Mvar	283.4 MW ,126.2 Mvar	283.4 MW ,126.2 Mvar

Preprints (www.preprints.org) | NOT PEER-REVIEWED | Posted: 17 September 2020 doi:10.20944/preprints202009.0373.v1

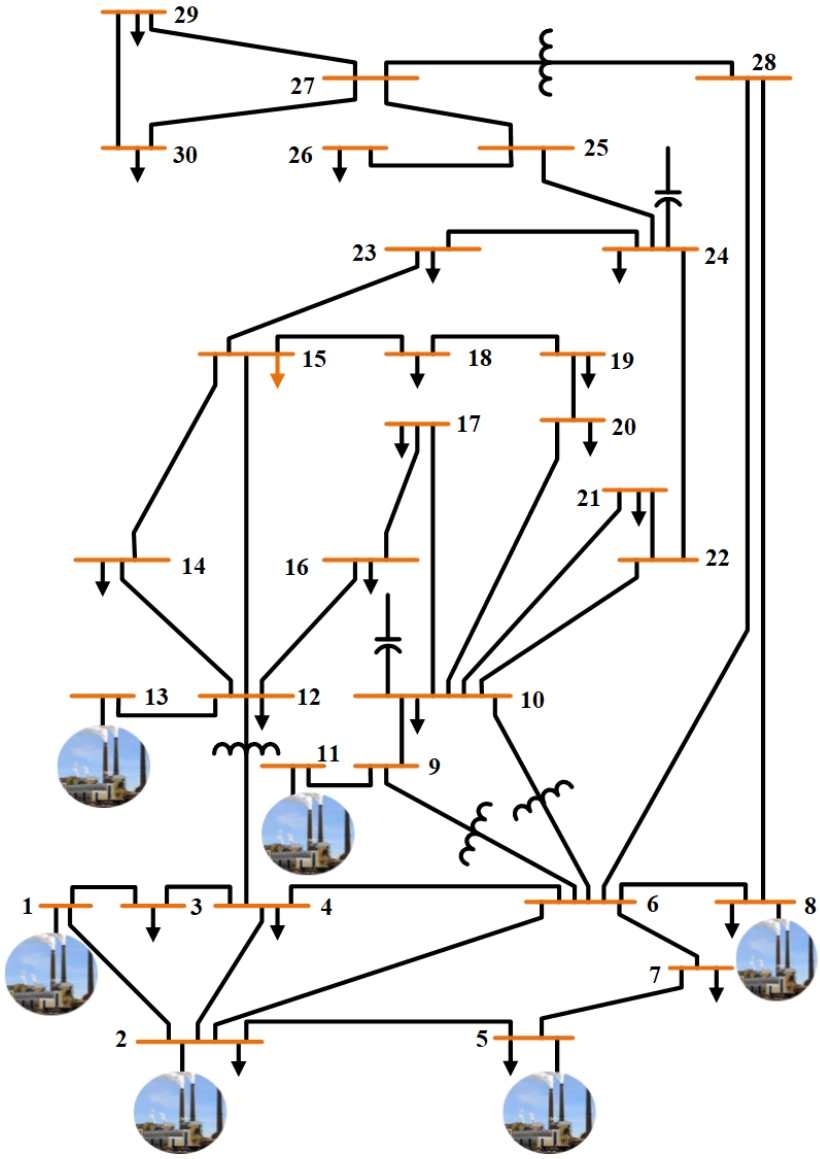

Figure 1. scenario 1: IEEE 30-bus system

- Test system 2: wind integrated IEEE 30-bus system
  In this system, the IEEE 30-bus system is modified by replacing the thermal power generating units at buses 5, 11, and13 with wind power generators. Moreover, new two wind generators have been added at buses 24, and 30, as seen in Figure 2 .The objective functions defined in Section2.2 is modified by adding the output power of wind plants ($P_w(v)$) given in Section 3. Case 3 and case 5 described in Section 2.2 are modified by adding the total cost of wind plants (C_T^w) defined in Section 3. The general specifications of this system and the data of wind power plants are given in Table 4 and Table 5, respectively.

Table 5. Data of wind power plant for test system 2.

Unit	Bus	No. of Turbines	P_{wr} [MW]	k	c	g_i [$/MWH]	$K_{Rw,i}$ [$/MWH]	$K_{Pw,i}$ [$/MWH]	v_{in} [m/s]	v_{out} [m/s]	v_r [m/s]
1	5	12	2	2	9	1.65	2.6	1.5	4	25	13
2	11	12	2	2	10	1.6	2.6	1.5	4	25	13
3	13	12	2	2	9	1.6	2.6	1.5	4	25	13
4	24	15	2	2	10	1.65	2.6	1.5	4	25	13
5	30	15	2	2	9	1.7	2.6	1.5	4	25	13

Preprints (www.preprints.org) | NOT PEER-REVIEWED | Posted: 17 September 2020 doi:10.20944/preprints202009.0373.v1

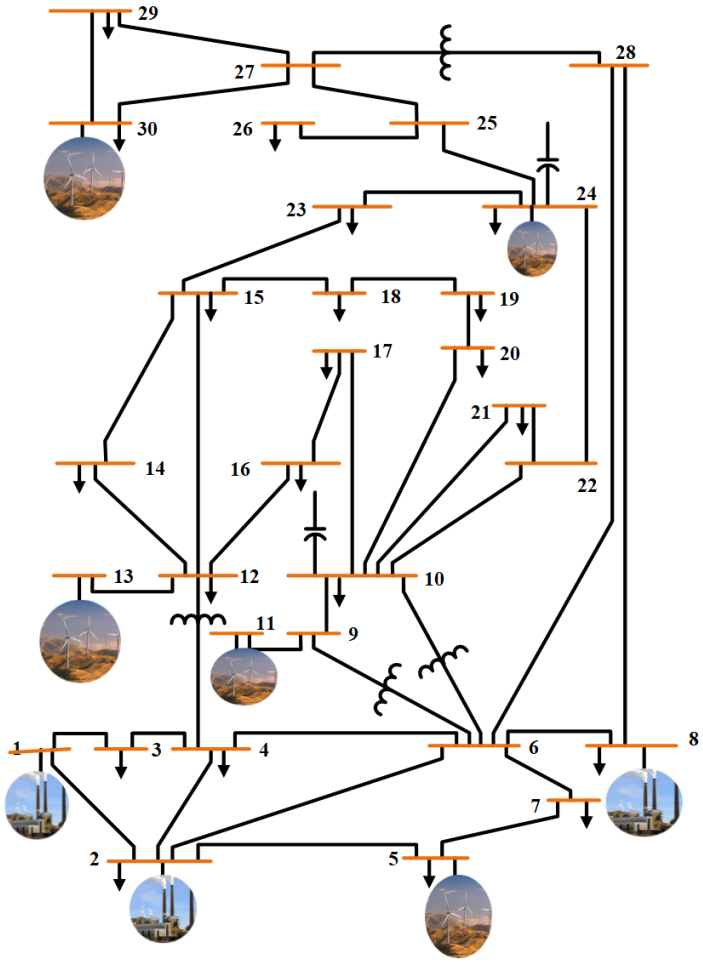

Figure 2. Wind integrated IEEE 30-bus system.

- Test system 3: Solar PV integrated IEEE 30-bus system
  This system is modified by locating solar PV generators at buses 5, 11, and13 instead of the thermal power generators. Furthermore, two new solar power generation units are installed at buses 24, and 30, as shown in Figure 3.The objective funtions defined in Section2.2 are modified by adding the output power of solar PV plants ($P_s(G)$) given in Section 3. Case 3 and case 5 described in Section 2.2 are modified by adding the total cost of solar PV plants (C_T^{PV}) defined in Section 3. The general data of this system and solar PV plants are presented in Table4 and Table 6, respectively.

Table 6. Data of solar power plant for test system 3.

Unit	Bus	P_{sr} [MW]	G_{std} [W/m^2]	R_c [W/m^2]	μ	σ	h_k [$/MWh]	$K_{Ps,k}$ [$/MWh]	$K_{Rs,k}$ [$/MWh]
1	5	24	800	170	6	0.6	1.55	3.2	1.3
2	11	24	800	200	6	0.6	1.45	2.8	1.3
3	13	24	800	170	6	0.6	1.6	3.1	1.45
4	24	30	800	170	6	0.6	1.6	3	1.3
5	30	30	800	200	6	0.6	1.6	3	1.3

Preprints (www.preprints.org) | NOT PEER-REVIEWED | Posted: 17 September 2020 doi:10.20944/preprints202009.0373.v1

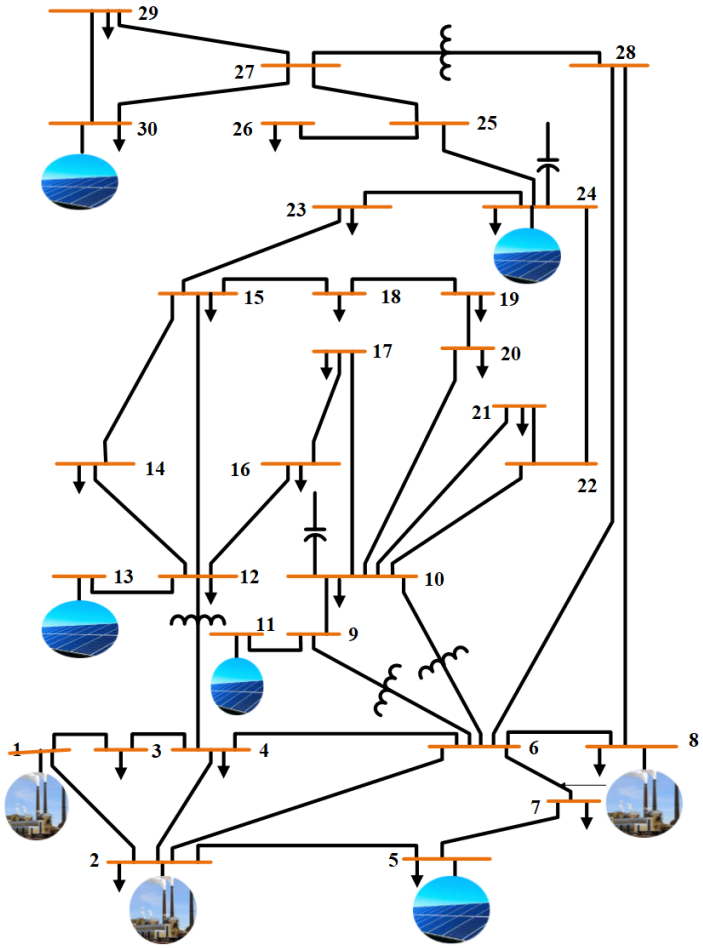

Figure 3. Solar PV integrated IEEE 30-bus system.

- Test system 4: Hybrid wind and solar PV integrated IEEE 30-bus system
  This modified test power system is simulated to show its behavior in the presence of both wind and solar PV power generating units, as depicted in Figure 4. The IEEE 30-bus system has been modified by replacing the thermal power generating units at buses 5, 11, and 13 with wind generator at bus 11 and solar PV at buses 5 and 13. In addition, the new solar PV and wind power generators are constructed at bus 24, and 30, respectively. The objective functions defined in Section2.2 are modified by adding the output power of solar PV plants ($P_s(G)$) and the output power of wind plants ($P_w(v)$) given in Section 3. Case 3 and case 5 described in Section 2.2 are modified by adding the total cost of solar PV plants (C_T^{PV}) and the total cost of wind plants (C_T^w) defined in Section 3. The specification of this hybrid power system is given in Table 4. The data of wind and solar PV plants are described in Table 7, and Table 8, respectively.

Table 7. Data of wind power plant for test system 4.

Unit	Bus	No. of Turbines	P_{wr} [MW]	k	c	g_i [$/MWH]	$K_{Rw,i}$ [$/MWH]	$K_{Pw,i}$ [$/MWH]	v_{in} [m/s]	v_{out} [m/s]	v_r [m/s]
1	11	12	2	2	9	1.7	2.8	1.7	4	25	13
2	30	12	2	2	10	1.7	2.8	1.7	4	25	13

Table 8. Data of solar power plant for test system 4.

Unit	**Bus**	P_{sr} **[MW]**	G_{std} **[W/m^2]**	R_c **[W/m^2]**	μ	σ	h_k **[$/MWh]**	$K_{Ps,k}$ **[$/MWh]**	$K_{Rs,k}$ **[$/MWh]**
1	5	24	800	170	6	0.6	1.55	3.2	1.3
2	13	30	800	170	6	0.6	1.45	3.1	1.45
3	30	30	800	200	6	0.6	1.6	3	1.3

Preprints (www.preprints.org) | NOT PEER-REVIEWED | Posted: 17 September 2020 doi:10.20944/preprints202009.0373.v1

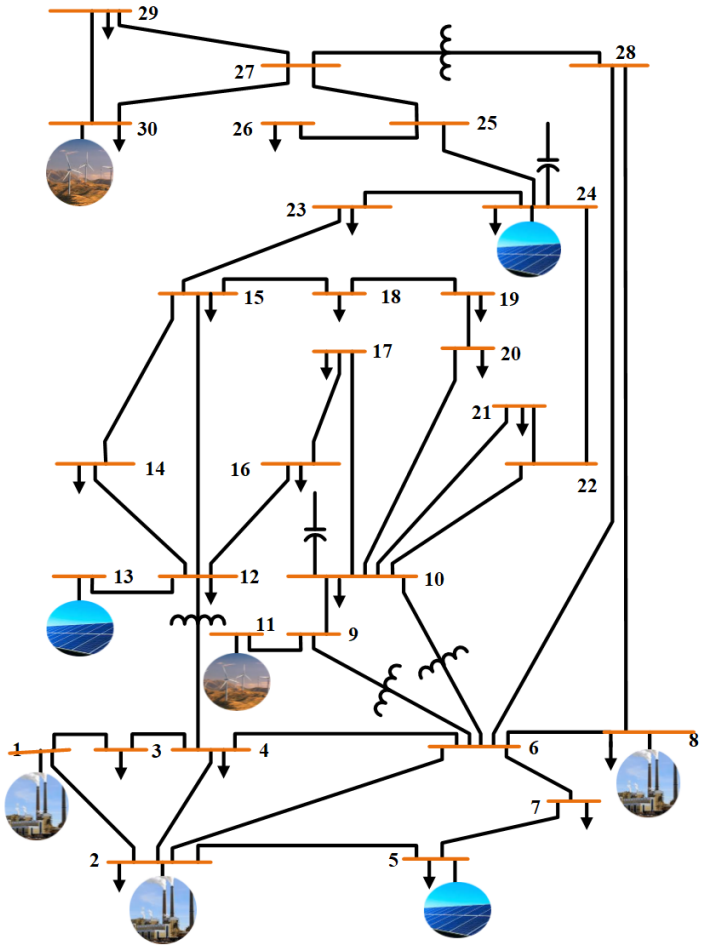

Figure 4. Hybrid wind and solar PV integrated IEEE 30-bus system.

6.2. Discussion and analysis of the objective functions of OPF

6.2.1. Minimization of real power loss

The EO [35], TLBO [45], MPSO [44], MFO [43], AGPSO1 [44], and TACPSO [44] algorithms are implemented on the test system 1, test system 2, test system 3, and test system 4 for the minimization of the real power loss as defined in Section 2.2. Fig. 5a shows the convergence characteristics of real power loss yielded by the best solution of the EO and other optimization methods for test system1. It observed that the better convergence characteristic is yielded by the EO. Furthermore, Fig. 5b and Fig.5c display voltage and loading profiles of test system1 for case 1. It is clear that the EO and other optimization methods obey the voltage limits of buses and loading limits of transmission lines. The results of EO and other techniques for test system 1 are displayed in Table 9

Table 9. Results of EO and other methods of case 1 for test system 1.

	MFO	TACPSO	AGPSO1	TLBO	EO	MPSO
VD (p.u.)	0.867649	0.898003	0.898362	0.87350728	0.917249	0.679794
FC ($/h)	967.4482	967.6206	967.6485	967.2492825	967.5865	967.7676
P_{loss} (MW)	3.124412	3.100891	3.094156	3.108417583	3.087342	3.144079
E (ton/h)	0.207299	0.207259	0.207266	0.207286164	0.207268	0.207273
f_o	3.124412	3.100891	3.094156	3.108417583	3.087342	3.144079

Preprints (www.preprints.org) | NOT PEER-REVIEWED | Posted: 17 September 2020 doi:10.20944/preprints202009.0373.v1

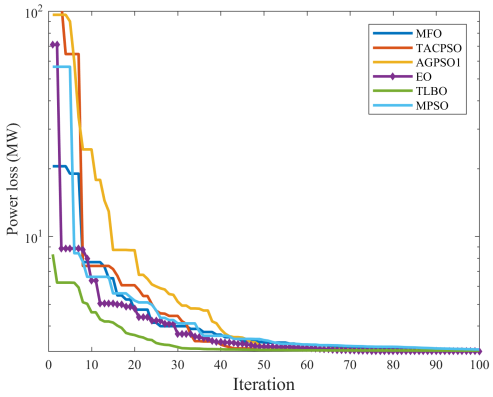

(a) Comparative convergence curves.

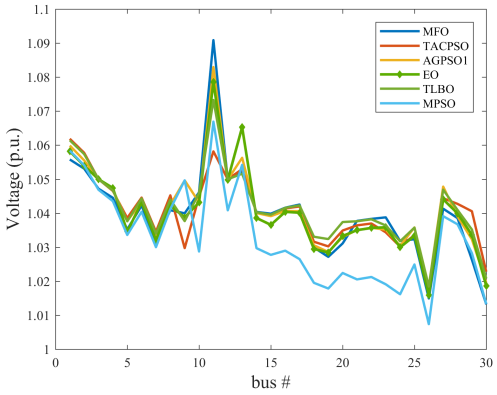

(b) Voltage profile.

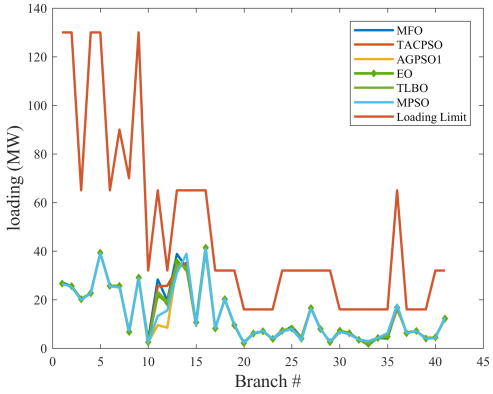

(c) Loading Profile

Figure 5. Comparative convergence, voltage and loading profiles for case 1 for all test systems.

The loss and loading profiles using EO for all test systems are given in Fig. 6.The optimal (best) results yielded by the EO method for the test system 1, test system 2, test system 3, and test system 4 are tabulated in Table 10.From Fig.6 and Table 10, it is seen that the losses of test system 2, test system 3, and test system 4 reduced by 23.6%, 31.52%, and 33.32%, respectively compared to test system 1.

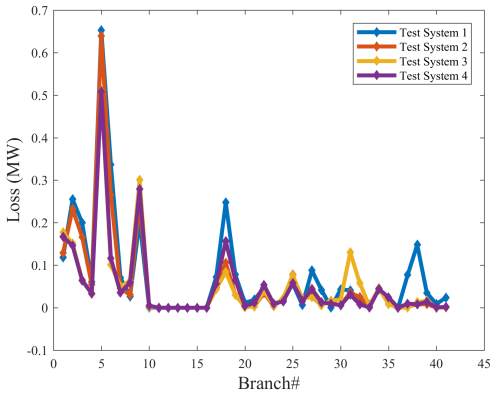

(a) Loss profile.

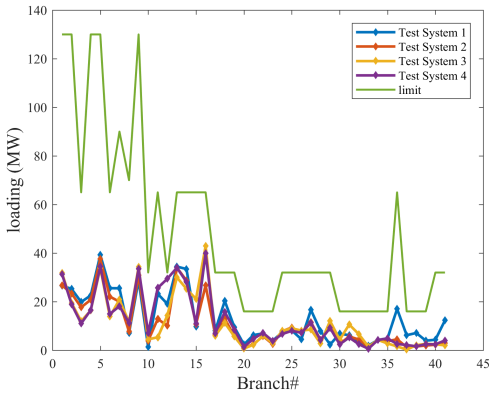

(b) Loading Profile

Figure 6. Loss and loading Profiles of case 1 for all test systems using EO.

Preprints (www.preprints.org) | NOT PEER-REVIEWED | Posted: 17 September 2020 doi:10.20944/preprints202009.0373.v1

Table 10. Optimal settings of control variables for case 1 for all test systems using EO.

Parameters	Min	Max	Test system 1	Test system 2	Test system 3	Test system 4
PG2 (MW)	20	80	79.9983006	72.14028714	48.22886744	51.07651611
PG5 (MW)	15	50	49.9982627	49.99945385	49.97347066	49.98470056
PG8 (MW)	10	35	34.99453958	26.20234283	34.77838714	34.92764479
PG11 (MW)	10	30	29.99984469	29.42347144	29.97517159	29.67713532
PG13 (MW)	10	40	39.99027741	25.72695297	29.69711674	39.69895071
PG24 (MW)	10	30		18.61010237	27.4148297	15.73782289
PG30 (MW)	10	40		13.58641689	15.23102984	14.35575851
V1 (p.u.)	0.95	1.1	1.061430345	1.033582214	1.037749499	1.056224426
V2 (p.u.)	0.95	1.1	1.057379791	1.027683624	1.032739079	1.051241045
V5 (p.u.)	0.95	1.1	1.037622078	1.003632229	1.013755431	1.032812731
V8 (p.u.)	0.95	1.1	1.044007621	1.015022765	1.02707043	1.045463882
V11 (p.u.)	0.95	1.1	1.073279794	1.063216144	0.999050197	1.042867188
V13 (p.u.)	0.95	1.1	1.051619936	1.034701938	1.044856898	1.020563172
V24 (p.u.)	0.95	1.1		1.024480465	1.009002895	1.020352939
V30 (p.u.)	0.95	1.1		1.022453184	1.018925985	1.040981535
QC10 (MVAr)	0	5	4.287709826	4.782286758	2.62406261	3.612693403
QC12 (MVAr)	0	5	2.093601675	0.000803534	0.986423834	2.416935212
QC15 (MVAr)	0	5	3.996488379	1.898614523	0.206692775	3.600783886
QC17 (MVAr)	0	5	4.136235738	4.356883849	2.716911629	0.342465282
QC20 (MVAr)	0	5	4.495134896	3.354513668	4.692404829	3.296807199
QC21 (MVAr)	0	5	5	0.046094293	2.038284465	0.872744865
QC23 (MVAr)	0	5	3.197386977	4.967912056	4.957773966	4.740324068
QC24 (MVAr)	0	5	4.806462479	4.536993047	3.79952116	3.698494945
QC29 (MVAr)	0	5	2.461175597	0.21865228	4.63994E-05	3.927880442
T11 (p.u.)	0.9	1.1	1.055740955	1.015687471	1.020034326	1.0962353
T12 (p.u.)	0.9	1.1	0.924042761	0.951998195	0.957069803	0.900424717
T15 (p.u.)	0.9	1.1	0.988530694	0.989254661	1.094558386	0.991494831
T36 (p.u.)	0.9	1.1	0.975749345	0.977273155	1.010207101	1.010623787
PG1 (MW)	50	200	51.50611659	50.08572807	50.22954768	50.01396753
QG1 (MVAr)	-20	150	-5.485983591	-1.712627012	-9.408754457	-4.363894439
QG2 (MVAr)	-20	60	7.574416698	7.129014137	3.920290677	9.504062082
QG5 (MVAr)	-15	62.5	21.13271229	17.01446382	19.68757038	20.6489489
QG8 (MVAr)	-15	48	26.41312254	26.16274206	28.52016815	33.06577869
QG11 (MVAr)	-10	40	19.21231862	19.38101083	0.13383456	18.93870787
QG13 (MVAr)	-15	44	2.247530335	8.029799729	33.49981989	-2.320248965
QG24 (MVAr)	-15	44		3.105401958	3.720374455	2.56415683
QG 30 (MVAr)	-15	44		0.296246809	2.993820748	1.368798025
VD **(p.u.)**			0.917249187	0.367181831	0.252949566	0.482190403
FC **($/h)**			967.5864625	417.7815499	358.1435956	368.1354088
P_{loss} **(MW)**			3.087341565	2.374755583	2.128420834	2.072496662
E **(ton/h)**			0.20726839	0.09655031	0.09111361	0.091202895
TC **($/h)**				863.2203104	823.476285	867.8385329
C_T^W **($/h)**				141.4837171		499.7031241
C_T^{PV} **($/h)**				303.9550435	465.3326895	
f_o **(MW)**			3.087341565	2.374755583	2.128420834	2.072496662

The statistical results (the best, the worst, the mean, and the standard deviation) of the real power loss for the EO and other optimization techniques are given in Table 11. As shown in Table 11, the minimum best, standard deviation, and mean are resulted from the EO.

Preprints (www.preprints.org) | NOT PEER-REVIEWED | Posted: 17 September 2020 doi:10.20944/preprints202009.0373.v1

Table 11. Summary of the statistical analysis of case 1 for test system 1.

	Best	Worst	Mean	Std dev
MFO	3.124412	3.469255	3.313791	0.115148
TACPSO	3.100891	3.495604	3.162984	0.119564
AGPSO1	3.094156	3.558659	3.136808	0.175963
TLBO	3.108418	3.271804	3.200392	0.057571
EO	3.087342	3.131426	3.089549	0.013218
MPSO	3.144079	3.417325	3.202598	0.080901

As expected, the addition and location of the renewable energy resources in the power system have a significant impact on reducing the real power loss.

6.2.2. Emission Index Minimization

In this case, the emission index defined in section 2.2 was minimized for all test systems. Fig. 7 demonstrates the convergence characteristics, loss profiles, and loading profiles for emission minimization using EO and other methods. It can be noticed from Fig. 7a that the EO has the smoothest and speediest convergence curves in comparing with other techniques, as well as Fig.7b and Fig.7c show that there is no violation in the voltage limits of buses and loading limits of transmission lines.

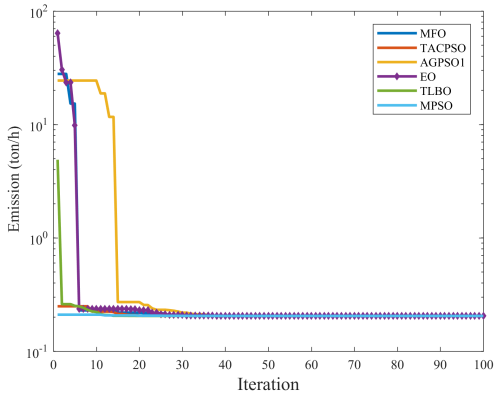

(a) Comparative convergence curves.

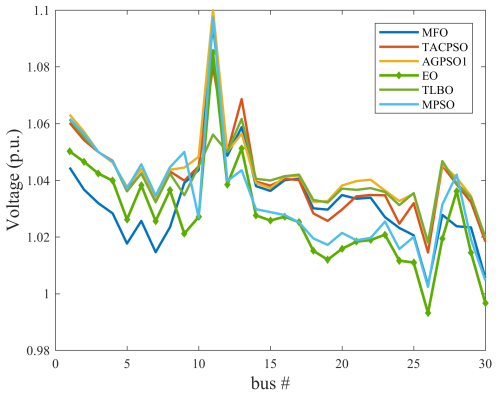

(b) Voltage profile.

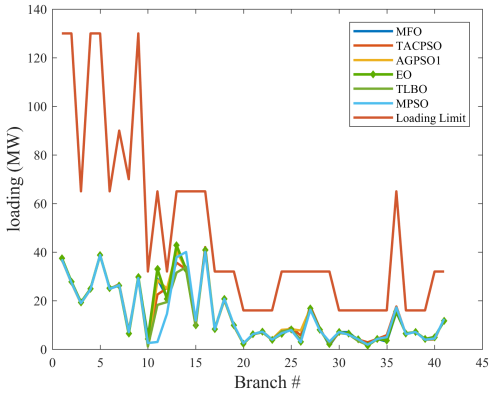

(c) Loading profile.

Figure 7. Comparative convergence ,voltage and loading Profiles for case 2 for all test systems.

Preprints (www.preprints.org) | NOT PEER-REVIEWED | Posted: 17 September 2020 doi:10.20944/preprints202009.0373.v1

The best (optimal) results obtained using the EO for all test systems for case 2 are shown in Table 12 .As we can see from Fig. 8 and Table 12 that emission index reduced by 55.54% for test system 2, test system 3, and test system 4 compared to test system 1.

Table 12. Optimal settings of control variables for case2 for all test systems using EO.

Parameters	Min	Max	Test system 1	Test system 2	Test system 3	Test system 4
PG2 (MW)	20	80	67.52765352	47.15393481	46.93784062	46.74579811
PG5 (MW)	15	50	49.99976843	49.99997692	48.55695793	49.63943974
PG8 (MW)	10	35	34.99979715	34.99785564	35	34.99981323
PG11 (MW)	10	30	30	13.08937369	24.11263394	28.93951933
PG13 (MW)	10	40	39.99994042	39.97364116	38.90979918	31.15977654
PG24 (MW)	10	30		29.67649489	20.72363213	13.68967898
PG30 (MW)	10	40		22.06349364	22.1793691	32.00183302
V1 (p.u.)	0.95	1.1	1.0613919	1.035577033	1.017785294	1.007633877
V2 (p.u.)	0.95	1.1	1.055299891	1.03014784	1.009596473	0.99225379
V5 (p.u.)	0.95	1.1	1.036061646	0.975474909	0.982885915	0.966515297
V8 (p.u.)	0.95	1.1	1.042336524	0.994262522	0.996877809	0.970873143
V11 (p.u.)	0.95	1.1	1.056098162	0.99155371	1.066472978	1.018197794
V13 (p.u.)	0.95	1.1	1.061630874	1.045591502	1.053301428	0.990382535
V24 (p.u.)	0.95	1.1		0.994310052	1.023161602	1.006430427
V30 (p.u.)	0.95	1.1		0.976743321	0.962066536	0.995194145
QC10 (MVAr)	0	5	4.194820255	0.691891638	0	2.28917862
QC12 (MVAr)	0	5	0.527663733	3.89808945	4.781805725	0.003693677
QC15 (MVAr)	0	5	4.925786364	0.093781976	4.681393138	3.767863825
QC17 (MVAr)	0	5	4.982842903	2.766984513	4.998326488	4.887538377
QC20 (MVAr)	0	5	4.671024822	4.426843395	4.610963598	5
QC21 (MVAr)	0	5	4.976075346	1.329009086	4.940763823	2.759967479
QC23 (MVAr)	0	5	2.74762835	3.54838243	0.002439547	4.271161763
QC24 (MVAr)	0	5	4.992557282	0.606928317	0.970384621	2.50397663
QC29 (MVAr)	0	5	2.088379542	4.949034272	0.000438444	2.957731038
T11 (p.u.)	0.9	1.1	1.045594251	0.951879814	0.938502294	0.940072546
T12 (p.u.)	0.9	1.1	0.921878284	0.962206441	1.096587454	0.919312335
T15 (p.u.)	0.9	1.1	1.00248085	1.099174642	1.018026147	1.023627655
T36 (p.u.)	0.9	1.1	0.972355171	0.92579926	1.099689643	1.060629423
PG1 (MW)	50	200	64.09434175	50.00003511	50.00023516	50.00000501
QG1 (MVAr)	-20	150	-5.544691231	0.054641352	-1.33241509	18.58616272
QG2 (MVAr)	-20	60	6.45002148	47.44923402	4.202024706	1.97952536
QG5 (MVAr)	-15	62.5	21.67156016	-1.442938766	13.43474762	19.83503047
QG8 (MVAr)	-15	48	27.29675405	23.11453954	7.583267029	12.95707181
QG11 (MVAr)	-10	40	11.72500454	-6.137543909	13.66528344	1.654000716
QG13 (MVAr)	-15	44	9.840166661	39.23629311	21.68524583	6.151027816
QG24 (MVAr)	-15	44		1.089772208	24.29742231	20.10756016
QG 30 (MVAr)	-15	44		-13.49116551	0.162345045	0.721702425
VD **(p.u.)**			0.9004031	0.298468513	0.404641642	0.391340877
FC**($/h)**			944.2808599	354.7638857	354.038595	353.3864113
P_{loss} **(MW)**			3.22150126	3.554805885	3.020468191	3.775864192
E **(ton/h)**			0.204818699	0.091061921	0.091060623	0.091060048
TC **($/h)**				877.5739313	865.4758094	867.8663197
C_T^W **($/h)**				108.3986993		514.4799085
C_T^{PV} **($/h)**				414.4113463	511.4372144	
f_o **(ton/h)**			0.204818699	0.091061921	0.091060623	0.091060048

Preprints (www.preprints.org) | NOT PEER-REVIEWED | Posted: 17 September 2020 doi:10.20944/preprints202009.0373.v1

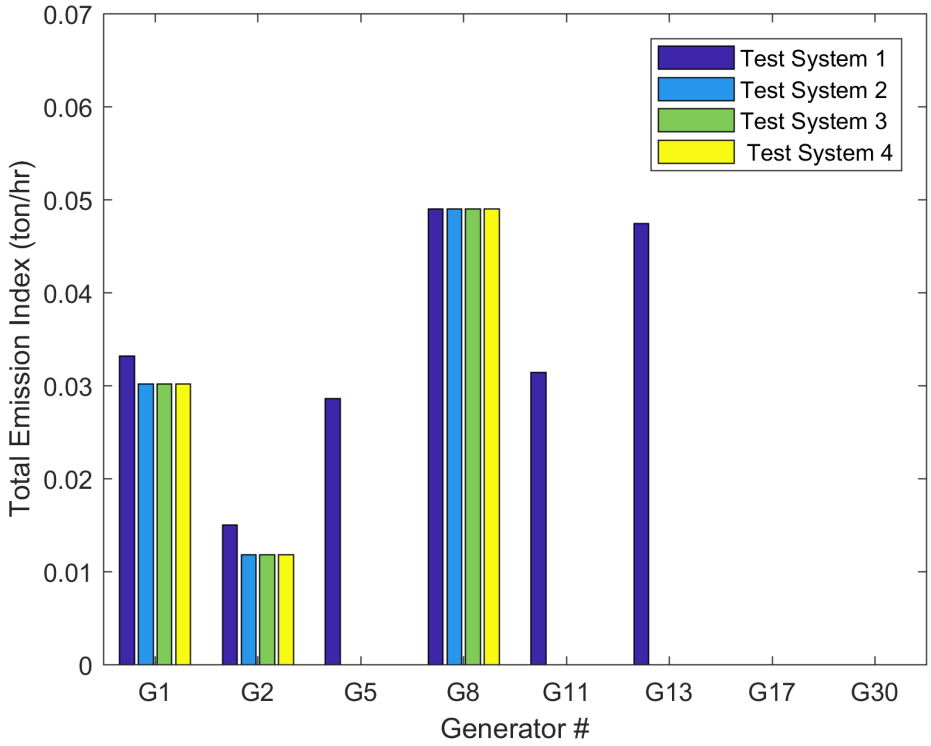

Figure 8. Total Emission index (ton/hr) of case 2 for all test systems using EO.

Table 13 summarizes the statistical results for the present case. It can be found from Table 13 that the EO provides the smallest best, standard deviation, and median than other methods.

Table 13. Summary of the statistical analysis of case 2 for test system 1.

	Best	Worst	Mean	Std dev
MFO	0.204862	0.204997	0.20495	4.15E-05
TACPSO	0.204839	0.205089	0.204943	9.14E-05
AGPSO1	0.204823	0.204999	0.204921	5.14E-05
TLBO	0.204855	0.204931	0.204892	2.43E-05
EO	0.204819	0.204878	0.204834	1.78E-05
MPSO	0.204833	0.20497	0.204934	5.44E-05

Table 14 presents the results of the EO and other methods for test system 1 with the minimization of emission index. For example, the objective function of case 2 for EO was 0.204819 ton/h compared to 0.204862 ton/h and 0.204885 ton/h for MFO [43] and TLBO [45] algorithms, respectively.

Table 14. Results of EO and other methods of case 2 for test system 1.

	MFO	TACPSO	AGPSO1	TLBO	EO	MPSO
VD (p.u.)	0.702001	0.856848	0.921129	0.541768425	0.900403	0.661504
FC ($/h)	944.3434	944.6554	944.3977	944.6873755	944.2809	944.4382
P_{loss} (MW)	3.356033	3.286856	3.235581	3.336091467	3.221501	3.267419
E (ton/h)	0.204862	0.204839	0.204823	0.204854728	0.204819	0.204833
f_o (ton/h)	0.204862	0.204839	0.204823	0.204854728	0.204819	0.204833

Preprints (www.preprints.org) | NOT PEER-REVIEWED | Posted: 17 September 2020 doi:10.20944/preprints202009.0373.v1

6.2.3. Minimization of the total cost of generating units

The comparative convergence characteristics, loading profiles, and loss profiles for test system 1 for the EO and other optimization techniques are presented in Fig.9. As observed in Fig.9, the voltage and loading profiles are kept within the acceptable ranges and the EO gives the best convergence characteristics compared to other methods. The optimal results of the EO and other techniques for test system 1 are summarized in Table 15. From Table 15, the EO leads to 800.4486$/hr total cost of generators which is better than the total cost obtained by the other compared methods.

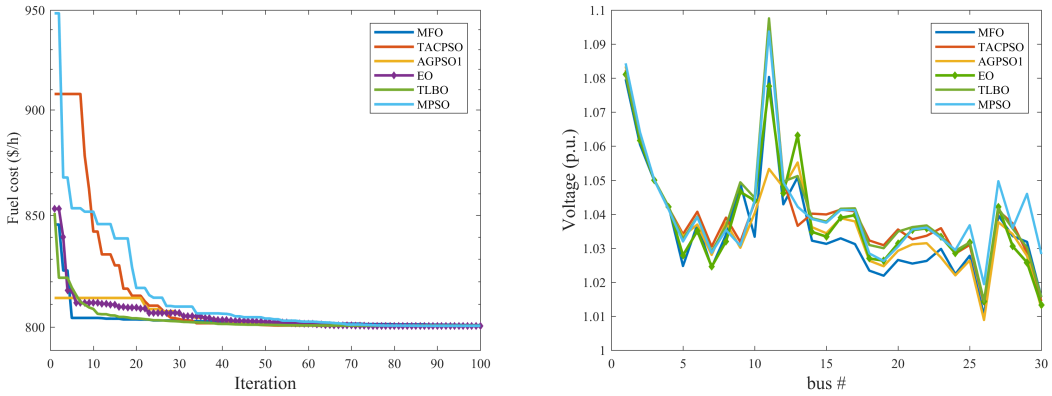

(a) Comparative convergence curves.

(b) Voltage profile.

(c) Loading Profile

Figure 9. Comparative convergence, voltage and loading Profiles for case 3 for all test systems.

Table 15. Results of EO and other methods of case 3 for test system 1.

	MFO	TACPSO	AGPSO1	TLBO	EO	MPSO
VD (p.u.)	0.740965	0.845878	0.761669	0.811019872	0.865075	0.877139
FC ($/h)	800.8283	800.5201	800.5595	800.616176	800.4486	800.5346
P_{loss} (MW)	9.134902	9.02898	9.040104	8.97569702	9.041464	9.059254
E (ton/h)	0.366492	0.366315	0.365967	0.363482104	0.367478	0.366949
f_o ($/h)	800.8283	800.5201	800.5595	800.616176	800.4486	800.5346

The statistical results yielded by the EO and other optimization techniques are given in Table16.

Preprints (www.preprints.org) | NOT PEER-REVIEWED | Posted: 17 September 2020 doi:10.20944/preprints202009.0373.v1

Table 16. Summary of the statistical analysis of case 3 for test system 1.

	Best	Worst	Mean	Std dev
MFO	800.8283	802.8078	801.5102	0.72899
TACPSO	800.5201	804.0448	800.6766	1.305504
AGPSO1	800.5595	802.1145	800.7023	0.453581
TLBO	800.6162	802.225	800.8366	0.471362
EO	800.4486	800.646	800.4793	0.057894
MPSO	800.5346	804.6442	801.1155	1.810857

From Table 17 and Fig.10, it can be observed that the total cost of generating units for test system 2, test system 3, and test system 4 declined by 3.54%, 3.47%, and 2.91%, respectively compared to test system 1.

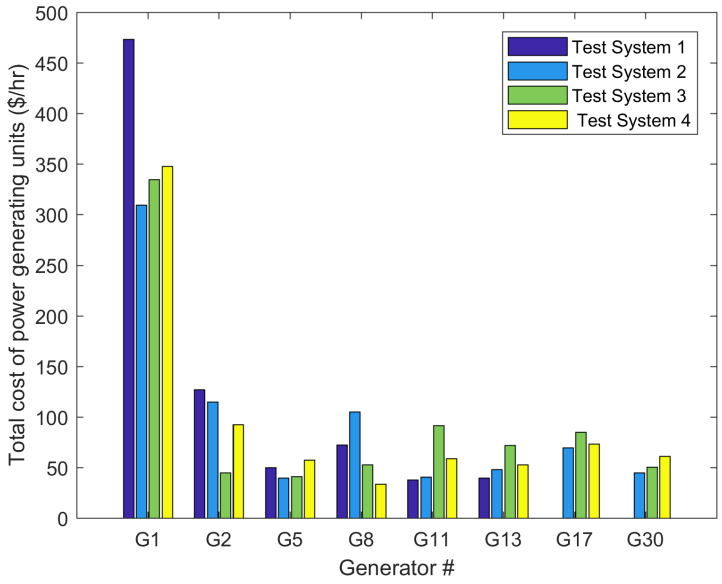

Figure 10. Total cost of generating units of case 3 for all test systems using EO.

Preprints (www.preprints.org) | NOT PEER-REVIEWED | Posted: 17 September 2020 doi:10.20944/preprints202009.0373.v1

Table 17. Optimal settings of control variables for case 3 for all test systems using EO.

Parameters	Min	Max	Test system 1	Test system 2	Test system 3	Test system 4
PG2 (MW)	20	80	48.74605575	45.18712121	21.21838812	38.17119779
PG5 (MW)	15	50	21.4315437	15.00195728	15.40668673	19.095538
PG8 (MW)	10	35	21.18353338	29.97018297	15.60913424	10.08641797
PG11 (MW)	10	30	11.52952165	13.07275916	29.402226	20.7452611
PG13 (MW)	10	40	12.0107829	19.71387022	30.51540057	17.9328134
PG24 (MW)	10	30		27.19702311	26.3304831	25.32965431
PG30 (MW)	10	40		14.74139467	17.72178713	20.28023584
V1 (p.u.)	0.95	1.1	1.081191705	1.022713246	1.02314065	1.059255936
V2 (p.u.)	0.95	1.1	1.063110135	1.006065736	1.008766945	1.043719467
V5 (p.u.)	0.95	1.1	1.032684857	0.956733982	0.961917138	1.009460201
V8 (p.u.)	0.95	1.1	1.036543249	0.994159517	0.985269141	1.02095678
V11 (p.u.)	0.95	1.1	1.097591909	1.012587735	1.049992902	1.0845661
V13 (p.u.)	0.95	1.1	1.051244633	1.054638289	1.011514979	1.046208927
V24 (p.u.)	0.95	1.1		1.035583887	1.011800496	1.043496784
V30 (p.u.)	0.95	1.1		0.95	0.996591531	1.048407181
QC10 (MVAr)	0	5	2.971616423	3.739491269	4.902790106	0.325756054
QC12 (MVAr)	0	5	0.655177618	4.809891924	1.662706176	3.06145818
QC15 (MVAr)	0	5	3.197516308	0.002648509	0.249875162	3.301750446
QC17 (MVAr)	0	5	4.723716655	3.279961844	1.827574807	1.707154585
QC20 (MVAr)	0	5	3.650622268	0.917150962	1.107119341	0.418013886
QC21 (MVAr)	0	5	5	4.948708899	2.08610321	4.893042007
QC23 (MVAr)	0	5	2.498554056	4.535914953	4.240774401	3.58924067
QC24 (MVAr)	0	5	4.985418463	5	0	1.169769378
QC29 (MVAr)	0	5	2.584313587	4.144114834	4.95463484	1.500067393
T11 (p.u.)	0.9	1.1	1.027284076	1.048412041	1.099843892	0.985023037
T12 (p.u.)	0.9	1.1	0.971275895	0.9	0.922169184	0.989956238
T15 (p.u.)	0.9	1.1	0.972373363	1.002944153	1.006664961	0.991751478
T36 (p.u.)	0.9	1.1	0.9815263	1.059841992	0.944073975	0.971316876
PG1 (MW)	50	200	177.5400261	125.374001	133.7249716	138.0708394
QG1 (MVAr)	-20	150	-0.570024945	-0.833938199	-5.669301771	-1.647701957
QG2 (MVAr)	-20	60	19.80925666	13.30674022	30.0465083	18.91158888
QG5 (MVAr)	-15	62.5	25.58480054	6.160576051	11.07617293	21.00268292
QG8 (MVAr)	-15	48	23.28431397	23.75265502	14.5584729	21.65678972
QG11 (MVAr)	-10	40	25.55139519	8.157153402	35.09222447	19.52230631
QG13 (MVAr)	-15	44	1.335643081	21.55072062	12.13070192	7.287213883
QG24 (MVAr)	-15	44		22.34214251	15.27252587	8.101017671
QG 30 (MVAr)	-15	44		-5.331414964	-8.278410983	-1.403218975
VD **(p.u.)**			0.865074691	0.312619858	0.288839815	0.653856503
FC **($/h)**			800.4486031	529.3973749	432.2815387	473.5571537
P_{loss} **(MW)**			9.041463508	6.858309749	6.529077621	6.311958209
E **(ton/h)**			0.367478227	0.141650437	0.159248156	0.163097259
TC **($/h)**				772.2465456	772.781097	777.3121394
C_T^W **($/h)**				85.46692162		303.7549857
C_T^{PV} **($/h)**				157.3822491	340.4995583	
f_o **($/h)**			800.4486031	772.2465456	772.781097	777.3121394

Preprints (www.preprints.org) | NOT PEER-REVIEWED | Posted: 17 September 2020 doi:10.20944/preprints202009.0373.v1

6.2.4. Voltage Deviation Minimization

Fig.11 demonstrates the voltage profiles for all test systems for this case using EO.The optimal solution obtained by EO for test system 1, test system 2, test system 3, and test system 4 are tabulated in Table 18. As shown in Fig.11 and Table 18, the presence of the renewable energy resources improves the voltage profiles and reduced the voltage deviation for test system 2, test system 3, and test system 4 by 22.46% ,37.39%,and 29.61% , respectively compared to test system1.

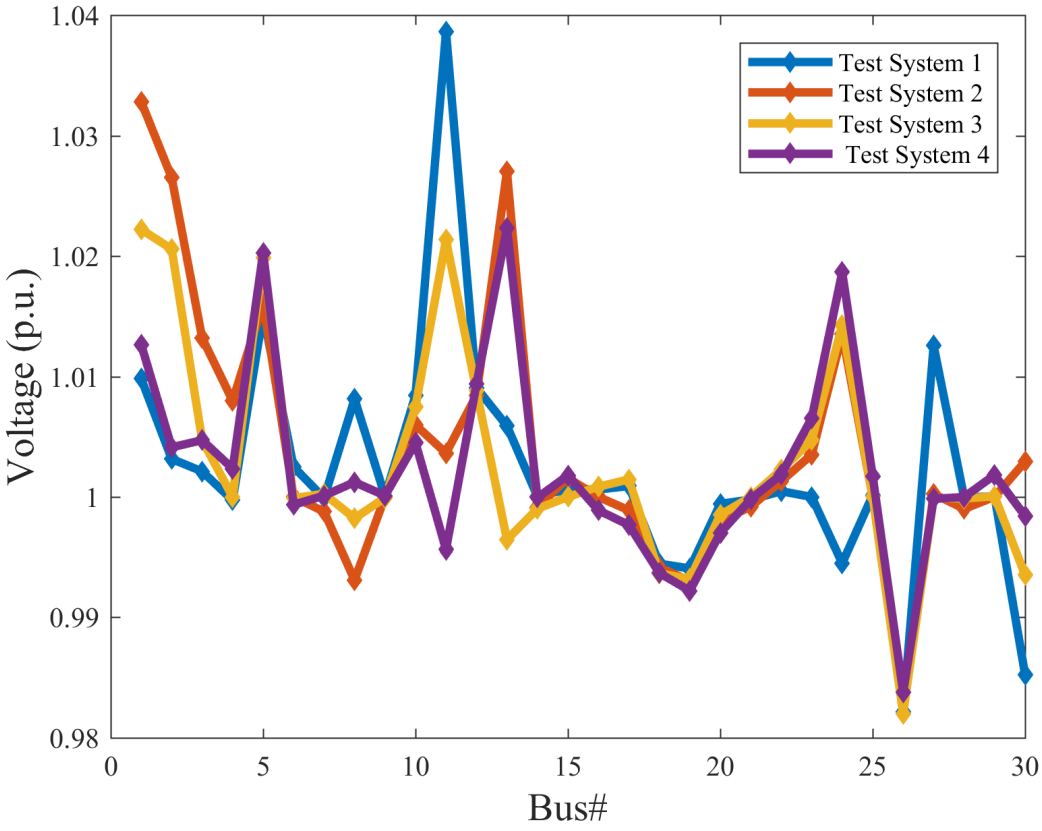

Figure 11. Voltage profiles of case 4 for all test systems using EO.

Preprints (www.preprints.org) | NOT PEER-REVIEWED | Posted: 17 September 2020 doi:10.20944/preprints202009.0373.v1

Table 18. Optimal settings of control variables for case 4 for all test systems using EO.

Parameters	Min	Max	Test system 1	Test system 2	Test system 3	Test system 4
PG2 (MW)	20	80	70.18121441	35.84850999	73.22346542	42.82238053
PG5 (MW)	15	50	25.52703119	20.27116158	33.56379457	47.02961201
PG8 (MW)	10	35	28.87890546	17.61889372	18.04097353	33.85695266
PG11 (MW)	10	30	29.30401557	24.63092203	10.13966121	14.67013887
PG13 (MW)	10	40	27.92172576	15.28698582	21.57955174	39.93831108
PG24 (MW)	10	30		16.34156919	10.07569951	28.44997135
PG30 (MW)	10	40		26.43024961	24.9797807	28.73744876
V1 (p.u.)	0.95	1.1	1.009811989	1.032801388	1.022207169	1.012647301
V2 (p.u.)	0.95	1.1	1.0031535	1.026505843	1.020581934	1.004121334
V5 (p.u.)	0.95	1.1	1.015213206	1.016105476	1.019877057	1.020275353
V8 (p.u.)	0.95	1.1	1.008124785	0.993094249	0.998231049	1.001227396
V11 (p.u.)	0.95	1.1	1.038640051	1.003641057	1.02134836	0.99563608
V13 (p.u.)	0.95	1.1	1.005894818	1.02703208	0.996453698	1.022325949
V24 (p.u.)	0.95	1.1		1.013528762	1.014235434	1.018656779
V30 (p.u.)	0.95	1.1		1.002929877	0.993533496	0.998414844
QC10 (MVAr)	0	5	4.9994342	1.057601365	4.449085771	1.224696754
QC12 (MVAr)	0	5	4.602398118	2.55410853	4.99999823	2.663316679
QC15 (MVAr)	0	5	4.960424711	4.999607248	1.610176653	3.415934203
QC17 (MVAr)	0	5	0.01181544	0.217347144	1.996228043	0.019033266
QC20 (MVAr)	0	5	4.996883927	4.92956648	4.978309396	4.994054795
QC21 (MVAr)	0	5	4.956429831	1.646590977	0.034134918	4.819904248
QC23 (MVAr)	0	5	4.972309922	0.427048793	1.956957345	1.039869954
QC24 (MVAr)	0	5	4.980435681	2.406207968	4.614781826	0.613094925
QC29 (MVAr)	0	5	2.520824595	1.71349761	3.890942901	3.740081954
T11 (p.u.)	0.9	1.1	1.056622635	1.012874303	1.035801681	1.002332018
T12 (p.u.)	0.9	1.1	0.901402975	0.900602964	0.902285005	0.901103808
T15 (p.u.)	0.9	1.1	0.981060937	1.013218403	0.960787866	0.998733169
T36 (p.u.)	0.9	1.1	0.966944023	0.987755959	0.989855906	0.98143194
PG1 (MW)	50	200	108.1160533	133.9296827	97.60688393	51.45175998
QG1 (MVAr)	-20	150	-19.10239902	-19.59757178	-19.11821266	-0.518817877
QG2 (MVAr)	-20	60	-14.85253038	31.85856685	18.90601653	-16.64972076
QG5 (MVAr)	-15	62.5	57.49581183	49.60698522	51.42002978	56.50571855
QG8 (MVAr)	-15	48	45.23093447	11.80532985	26.14354452	31.44056819
QG11 (MVAr)	-10	40	20.12674964	2.380585374	10.62092072	-1.914317997
QG13 (MVAr)	-15	44	-1.74441538	13.80317636	-8.465359993	10.55389137
QG24 (MVAr)	-15	44		14.86630972	15.99035449	13.88576475
QG 30 (MVAr)	-15	44		-4.888937122	-7.68659143	-7.960636408
VD **(p.u.)**			0.088397534	0.08005165	0.064632335	0.07266919
FC **($/h)**			848.7795548	480.1984844	514.2584395	339.455916
P_{loss} **(MW)**			6.528945889	6.957974748	5.809810669	3.556575273
E **(ton/h)**			0.240505607	0.155665569	0.119726864	0.091393798
TC **($/h)**				787.9483007	810.1863986	861.8303756
C_T^W **($/h)**				164.040337		522.3744597
C_T^{PV} **($/h)**				143.7094792	295.9279591	
f_o **(p.u.)**			0.088397534	0.08005165	0.064632335	0.07266919

311 It is clear from Table 19; the minimum best, standard deviation, and median are obtained by the EO.

Preprints (www.preprints.org) | NOT PEER-REVIEWED | Posted: 17 September 2020 doi:10.20944/preprints202009.0373.v1

Table 19. Summary of the statistical analysis of case 4 for test system 1.

	Best	Worst	Mean	Std dev
MFO	0.100862	0.137899	0.117452	0.011555
TACPSO	0.092725	0.177792	0.116202	0.025827
AGPSO1	0.102816	0.144276	0.131944	0.01565
TLBO	0.103244	0.152343	0.112717	0.015185
EO	0.088398	0.097568	0.092814	0.002809
MPSO	0.093414	0.202628	0.124612	0.038641

From Fig.12, the voltage and loading profiles for this case for all optimization methods obey the constraints of voltages at load buses and transmission line loading. It can be also observed that the EO convergence characteristic outperforms the convergence characteristics of other methods. The results of EO and other methods for test system 1 are given in Table 20.

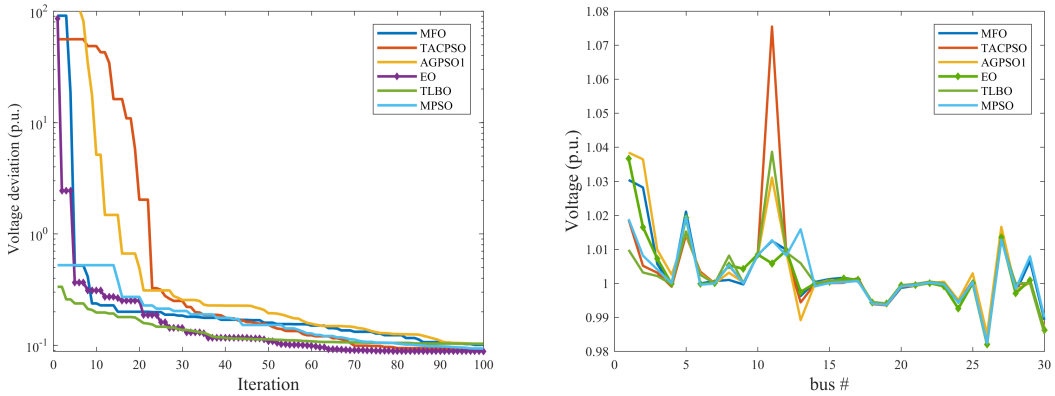

(a) Comparative convergence curves.

(b) Voltage profile.

(c) Loading Profile

Figure 12. Comparative convergence, voltage and loading profiles for case 4 for all test systems.

Preprints (www.preprints.org) | NOT PEER-REVIEWED | Posted: 17 September 2020 doi:10.20944/preprints202009.0373.v1

Table 20. Results of EO and other methods of case 4 for test system 1.

	MFO	TACPSO	AGPSO1	TLBO	EO	MPSO
VD (p.u.)	0.100862	0.092725	0.102816	0.103243696	0.088398	0.093414
FC ($/h)	901.7397	852.0642	834.1079	829.5879108	848.7796	841.3429
P_{loss} (MW)	5.965677	9.980964	7.492151	8.391654887	6.528946	7.564352
E (ton/h)	0.248497	0.359732	0.273799	0.337325958	0.240506	0.275282
f_o (p.u.)	0.100862	0.092725	0.102816	0.103243696	0.088398	0.093414

6.2.5. Case 5: Minimization of the total cost of the generating units, voltage deviation, real power loss, and emission index

It is clear from Fig.13, the EO has the best convergence characteristics compared to the other optimization algorithms and the voltage and loading profiles for all algorithms ranges within the allowable limits. The results of EO and other methods for test system 1 of this case are shown in Table 21.

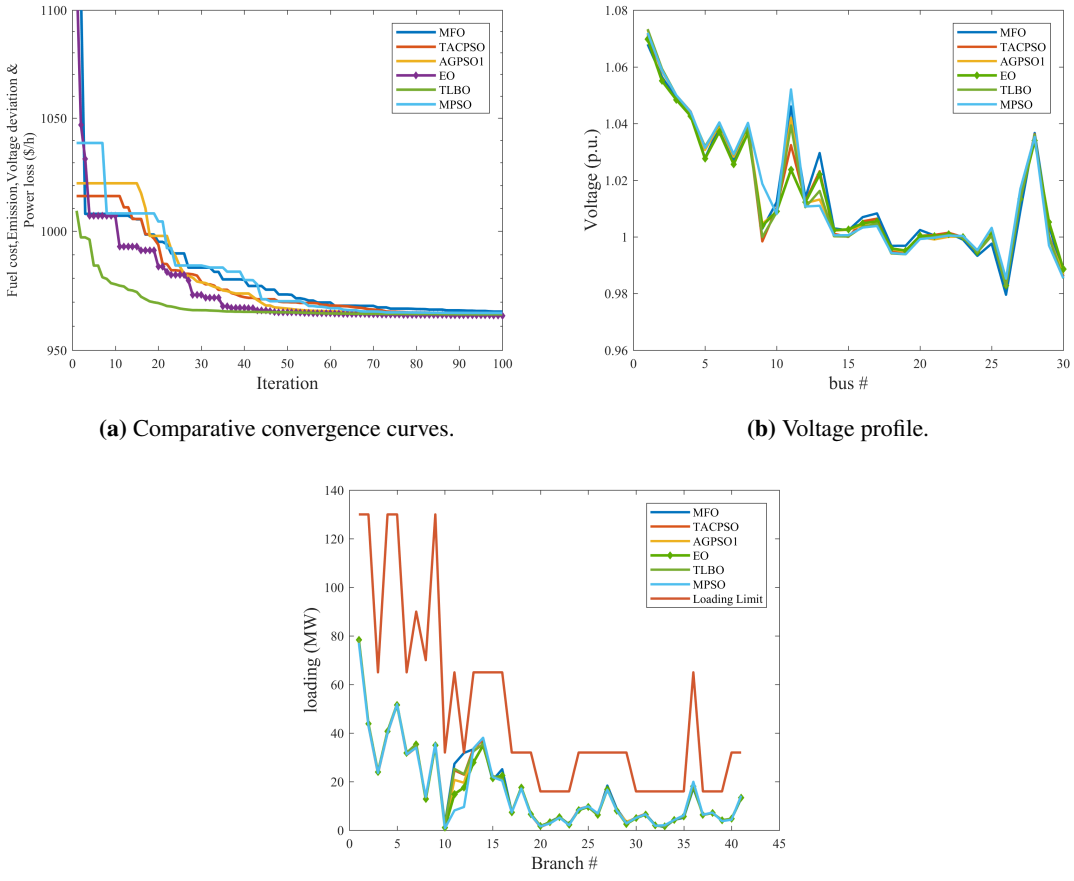

(a) Comparative convergence curves.

(b) Voltage profile.

(c) Loading profile.

Figure 13. Comparative convergence, voltage and loading profiles for case 5 for all test system 1.

Preprints (www.preprints.org) | NOT PEER-REVIEWED | Posted: 17 September 2020 doi:10.20944/preprints202009.0373.v1

Table 21. Results of EO and other methods of case 5 for test system 1.

	MFO	TACPSO	AGPSO1	TLBO	EO	MPSO
VD (p.u.)	0.312222	0.301092	0.2979	0.292001838	0.291525	0.315655
FC ($/h)	832.131	833.4427	831.8455	831.251448	829.9924	833.2358
P_{loss} (MW)	5.569804	5.471244	5.542919	5.575077257	5.604236	5.490564
E (ton/h)	0.250434	0.249973	0.251339	0.252691258	0.253454	0.249919
f_o ($/h)	965.9816	964.8825	964.8211	964.8363202	964.2232	965.4054

The statistical analysis of the EO and other methods for test system 1 are given in Table 22. As shown in table, the EO gives the minimum best, median and standard deviation.

Table 22. Summary of the statistical analysis of case 5 for test system 1.

	Best	Worst	Mean	Std dev
MFO	965.9816	970.7178	968.0071	1.616872
TACPSO	964.8825	968.5757	965.8415	1.251791
AGPSO1	964.8211	967.8093	965.6185	0.874411
TLBO	964.8363	968.0825	966.0087	1.105687
EO	964.2232	966.3464	964.5618	0.655197
MPSO	965.4054	978.9642	966.4455	4.054598

It is clear from Fig.14 and Table 23 that the objective function for this case for test system 2, test system 3, and test system 4 dropped by 3.90%, 7.77%, and 7.84%, respectively compared to test system1. It is found from Table 23 that the real power loss for test system 2, test system 3, and test system 4 dropped by 30.94%, 20.75%, and 46.06%, respectively compared to test system1.

Preprints (www.preprints.org) | NOT PEER-REVIEWED | Posted: 17 September 2020 doi:10.20944/preprints202009.0373.v1

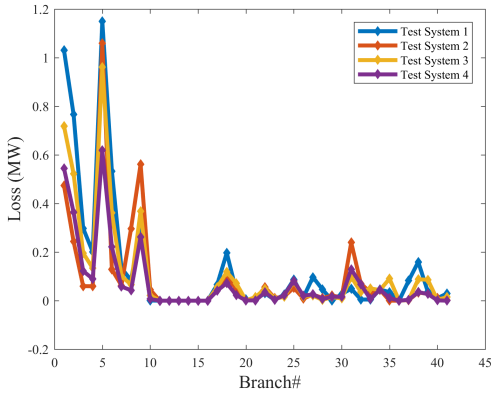

(a) Loss profile.

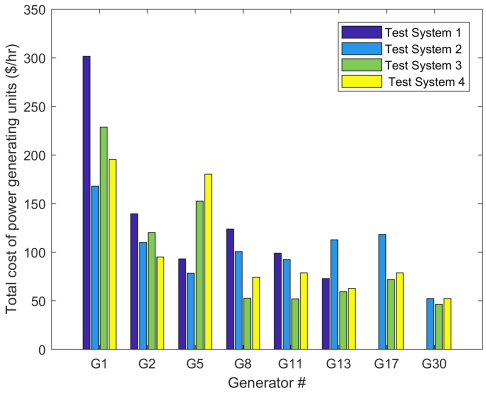

(b) Total cost of generating units.

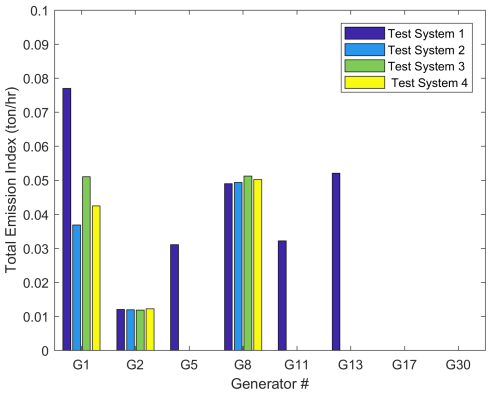

(c) Total emission index.

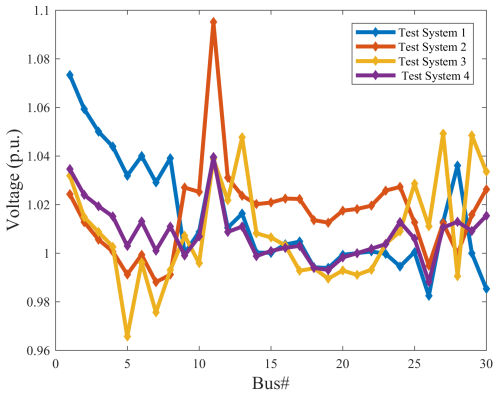

(d) Voltage profiles.

Figure 14. Total cost of generating units, total emission index, voltage and loss profiles of case 5 for all test systems.

Preprints (www.preprints.org) | NOT PEER-REVIEWED | Posted: 17 September 2020 doi:10.20944/preprints202009.0373.v1

Table 23. Optimal settings of control variables for case 5 for all test systems using EO.

Parameters	Min	Max	Test system 1	Test system 2	Test system 3	Test system 4
PG2 (MW)	20	80	52.34900301	43.76198174	46.85392201	39.04580002
PG5 (MW)	15	50	31.41892625	25.13957863	41.57764325	49.63341394
PG8 (MW)	10	35	34.99720302	28.83722988	15.57308058	21.63539649
PG11 (MW)	10	30	26.95716205	27.72005416	28.54767347	26.5299306
PG13 (MW)	10	40	20.69034077	37.30220041	21.35593529	20.93782021
PG24 (MW)	10	30		33.41823981	19.87429698	27.03669094
PG30 (MW)	10	40		17.31391519	17.29441758	17.27175615
V1 (p.u.)	0.95	1.1	1.073302714	1.024270078	1.031881955	1.034535652
V2 (p.u.)	0.95	1.1	1.05933056	1.012773005	1.014838234	1.023955028
V5 (p.u.)	0.95	1.1	1.031867076	0.991186486	0.965629646	1.002922115
V8 (p.u.)	0.95	1.1	1.039079245	0.991138879	0.993005954	1.010973253
V11 (p.u.)	0.95	1.1	1.039336016	1.1	1.038730973	1.039568814
V13 (p.u.)	0.95	1.1	1.016224258	1.023619922	1.047631647	1.010922024
V24 (p.u.)	0.95	1.1		1.027240201	1.008908379	1.012804196
V30 (p.u.)	0.95	1.1		1.026258901	1.033487159	1.015369168
QC10 (MVAr)	0	5	1.42704702	0.24222794	5	3.367347878
QC12 (MVAr)	0	5	0.114983911	4.465905221	5	4.957438998
QC15 (MVAr)	0	5	2.71927269	0	1.436680682	3.38628092
QC17 (MVAr)	0	5	4.777257639	4.971408287	0	4.999449612
QC20 (MVAr)	0	5	4.891165116	4.864936873	5	4.836689278
QC21 (MVAr)	0	5	4.917867343	4.114355205	4.252301174	2.729537609
QC23 (MVAr)	0	5	4.944826897	4.912774176	0	1.224294666
QC24 (MVAr)	0	5	4.999139393	3.383242169	2.790571405	4.901232863
QC29 (MVAr)	0	5	2.36221935	0.622641699	5	0.478740405
T11 (p.u.)	0.9	1.1	1.098277898	1.041847001	0.996768732	1.070613035
T12 (p.u.)	0.9	1.1	0.937769396	0.906411875	1.061448786	0.920185016
T15 (p.u.)	0.9	1.1	1.02148431	0.939592837	0.983885511	0.995441894
T36 (p.u.)	0.9	1.1	1.002153866	0.991006369	0.904079564	0.993400466
PG1 (MW)	50	200	122.5915999	73.77703	96.76396309	84.33186618
QG1 (MVAr)	-20	150	0.44760914	4.980415704	11.6826979	-1.350997342
QG2 (MVAr)	-20	60	13.45186855	10.12960773	16.17020662	8.009356413
QG5 (MVAr)	-15	62.5	22.96436543	30.2545861	-0.480850004	19.94798351
QG8 (MVAr)	-15	48	25.09929462	4.325252485	25.37843413	24.0097914
QG11 (MVAr)	-10	40	20.42841833	39.34377358	16.58858651	20.9433804
QG13 (MVAr)	-15	44	4.484753294	-4.510415315	19.67801235	1.913484758
QG24 (MVAr)	-15	44		-1.505790029	2.129992746	2.949992903
QG 30 (MVAr)	-15	44		3.138390036	-7.584798837	0.645488754
VD **(p.u.)**			0.291524702	0.340717958	0.287869453	0.142747756
FC **($/h)**			829.9923878	378.7198323	401.6872426	364.5623372
P_{loss} **(MW)**			5.604235892	3.870229887	4.440932453	3.022674546
E **(ton/h)**			0.253453881	0.098214148	0.114249163	0.104949647
TC **($/h)**				832.9987095	783.916446	817.6301115
C_T^W **($/h)**				144.7990782		453.0677743
C_T^{PV} **($/h)**				309.4797989	382.2292034	
f_o **($/h)**			964.2232199	927.1649129	889.8329526	889.1206976

7. Conclusions

In this study, a novel proposed EO method has been successfully applied to solve single and multi-objective OPF with integrated wind turbines and solar PV generators. Its performance and effectiveness were evaluated on four power system, namely: IEEE 30-bus system, wind integrated IEEE 30-bus system, solar PV integrated IEEE 30-bus system, and hybrid wind and solar PV integrated IEEE 30-bus system. Realistic models for the wind turbines and solar PV systems have been proposed and thus real power outputs of wind turbines and solar PV power plants have been accurately forecasted .Therefore, correct and efficient decision can be taken for inclusion the wind turbines and solar PV power plants in the proper locations. The simulation and statistical results indicate

Preprints (www.preprints.org) | NOT PEER-REVIEWED | Posted: 17 September 2020 doi:10.20944/preprints202009.0373.v1

and approve that the EO[35] method outperforms other optimization techniques ,namely: TLBO [45], MPSO [44], MFO [43], AGPSO1 [44], and TACPSO [44] .Our research has highlighted the importance of the proper locations of the renewable energy resources on improving the objective functions of OPF problem. Furthermore, adding wind turbines and solar PV play an integral role in enhancing the performance of the standard IEEE 30-bus system .For example, they significantly reduce the fuel cost and emission of the conventional power generators ,as well as minimize real power loss and voltage deviation .

Author Contributions: Both authors have made equal contributions to this work.

Funding: This research received no external funding.

Conflicts of Interest: The authors declare no conflict of interest.

References

1. Roy, R.; Jadhav, H. Optimal power flow solution of power system incorporating stochastic wind power using Gbest guided artificial bee colony algorithm. *International Journal of Electrical Power & Energy Systems* **2015**, *64*, 562–578.
2. Shi, L.; Wang, C.; Yao, L.; Ni, Y.; Bazargan, M. Optimal power flow solution incorporating wind power. *IEEE Systems Journal* **2011**, *6*, 233–241.
3. Biswas, P.P.; Suganthan, P.N.; Mallipeddi, R.; Amaratunga, G.A. Optimal reactive power dispatch with uncertainties in load demand and renewable energy sources adopting scenario-based approach. *Applied Soft Computing* **2019**, *75*, 616–632.
4. Biswas, P.P.; Suganthan, P.; Amaratunga, G.A. Optimal power flow solutions incorporating stochastic wind and solar power. *Energy Conversion and Management* **2017**, *148*, 1194–1207.
5. Dommel, H.; Tinney, W. 91968) Optimal Power Flow solutions IEEE Transactions on Power Apparatus and Systems, Vol. *PAS–87* **1866**, *1876*.
6. Jabr, R.A. Optimal power flow using an extended conic quadratic formulation. *IEEE transactions on power systems* **2008**, *23*, 1000–1008.
7. Lin, W.M.; Huang, C.H.; Zhan, T.S. A hybrid current-power optimal power flow technique. *IEEE Transactions on Power Systems* **2008**, *23*, 177–185.
8. Glavitsch, H.; Spoerry, M. Quadratic loss formula for reactive dispatch. *IEEE transactions on power apparatus and systems* **1983**, pp. 3850–3858.
9. Burchett, R.; Happ, H.; Wirgau, K. Large scale optimal power flow. *IEEE Transactions on Power Apparatus and Systems* **1982**, pp. 3722–3732.
10. Lobato, E.; Rouco, L.; Navarrete, M.; Casanova, R.; Lopez, G. An LP-based optimal power flow for transmission losses and generator reactive margins minimization. 2001 IEEE Porto Power Tech Proceedings (Cat. No. 01EX502). IEEE, 2001, Vol. 3, pp. 5–pp.
11. Duman, S.; Güvenç, U.; Sönmez, Y.; Yörükeren, N. Optimal power flow using gravitational search algorithm. *Energy Conversion and Management* **2012**, *59*, 86–95.
12. El Ela, A.A.; Abido, M.; Spea, S. Optimal power flow using differential evolution algorithm. *Electric Power Systems Research* **2010**, *80*, 878–885.
13. Bouchekara, H. Optimal power flow using black-hole-based optimization approach. *Applied Soft Computing* **2014**, *24*, 879–888.
14. Mohamed, A.A.A.; Mohamed, Y.S.; El-Gaafary, A.A.; Hemeida, A.M. Optimal power flow using moth swarm algorithm. *Electric Power Systems Research* **2017**, *142*, 190–206.
15. Hazra, J.; Sinha, A. A multi-objective optimal power flow using particle swarm optimization. *European transactions on electrical power* **2011**, *21*, 1028–1045.
16. Bhattacharya, A.; Roy, P. Solution of multi-objective optimal power flow using gravitational search algorithm. *IET generation, transmission & distribution* **2012**, *6*, 751–763.
17. Shabanpour-Haghighi, A.; Seifi, A.R.; Niknam, T. A modified teaching–learning based optimization for multi-objective optimal power flow problem. *Energy Conversion and Management* **2014**, *77*, 597–607.
18. Kumar, S.; Chaturvedi, D. Optimal power flow solution using fuzzy evolutionary and swarm optimization. *International Journal of Electrical Power & Energy Systems* **2013**, *47*, 416–423.

Preprints (www.preprints.org) | NOT PEER-REVIEWED | Posted: 17 September 2020 doi:10.20944/preprints202009.0373.v1

19. Khorsandi, A.; Hosseinian, S.; Ghazanfari, A. Modified artificial bee colony algorithm based on fuzzy multi-objective technique for optimal power flow problem. *Electric Power Systems Research* **2013**, *95*, 206–213.
20. Ghasemi, M.; Ghavidel, S.; Ghanbarian, M.M.; Gharibzadeh, M.; Vahed, A.A. Multi-objective optimal power flow considering the cost, emission, voltage deviation and power losses using multi-objective modified imperialist competitive algorithm. *Energy* **2014**, *78*, 276–289.
21. Narimani, M.R.; Azizipanah-Abarghooee, R.; Zoghdar-Moghadam-Shahrekohne, B.; Gholami, K. A novel approach to multi-objective optimal power flow by a new hybrid optimization algorithm considering generator constraints and multi-fuel type. *Energy* **2013**, *49*, 119–136.
22. Ghasemi, M.; Ghavidel, S.; Akbari, E.; Vahed, A.A. Solving non-linear, non-smooth and non-convex optimal power flow problems using chaotic invasive weed optimization algorithms based on chaos. *Energy* **2014**, *73*, 340–353.
23. Krishnanand, K.; Hasani, S.M.F.; Panigrahi, B.K.; Panda, S.K. Optimal power flow solution using self–evolving brain–storming inclusive teaching–learning–based algorithm. International Conference in Swarm Intelligence. Springer, 2013.
24. Sivasubramani, S.; Swarup, K. Sequential quadratic programming based differential evolution algorithm for optimal power flow problem. *IET generation, transmission & distribution* **2011**, *5*, 1149–1154.
25. Reddy, S.S. Optimal power flow with renewable energy resources including storage. *Electrical Engineering* **2017**, *99*, 685–695.
26. Shilaja, C.; Arunprasath, T. Optimal power flow using Moth Swarm Algorithm with Gravitational Search Algorithm considering wind power. *Future Generation Computer Systems* **2019**, *98*, 708–715.
27. Aien, M.; Fotuhi-Firuzabad, M.; Rashidinejad, M. Probabilistic optimal power flow in correlated hybrid wind–photovoltaic power systems. *IEEE Transactions on Smart Grid* **2014**, *5*, 130–138.
28. Aien, M.; Rashidinejad, M.; Firuz-Abad, M.F. Probabilistic optimal power flow in correlated hybrid wind-PV power systems: A review and a new approach. *Renewable and Sustainable Energy Reviews* **2015**, *41*, 1437–1446.
29. Liang, R.H.; Tsai, S.R.; Chen, Y.T.; Tseng, W.T. Optimal power flow by a fuzzy based hybrid particle swarm optimization approach. *Electric Power Systems Research* **2011**, *81*, 1466–1474.
30. Shilaja, C.; Ravi, K. Optimal power flow using hybrid DA-APSO algorithm in renewable energy resources. *Energy Procedia* **2017**, *117*, 1085–1092.
31. Biswas, P.P.; Suganthan, P.; Amaratunga, G.A. Optimal power flow solutions incorporating stochastic wind and solar power. *Energy Conversion and Management* **2017**, *148*, 1194–1207.
32. Das, T.; Roy, R.; Mandal, K.K.; Mondal, S.; Mondal, S.; Hait, P.; Das, M.K. Optimal Reactive Power Dispatch Incorporating Solar Power Using Jaya Algorithm. In *Computational Advancement in Communication Circuits and Systems*; Springer, 2020; pp. 37–48.
33. Chen, M.R.; Zeng, G.Q.; Lu, K.D. Constrained multi-objective population extremal optimization based economic-emission dispatch incorporating renewable energy resources. *Renewable Energy* **2019**, *143*, 277–294.
34. Rambabu, M.; Nagesh Kumar, G.; Sivanagaraju, S. Optimal Power Flow of Integrated Renewable Energy System using a Thyristor Controlled SeriesCompensator and a Grey-Wolf Algorithm. *Energies* **2019**, *12*, 2215.
35. Faramarzi, A.; Heidarinejad, M.; Stephens, B.; Mirjalili, S. Equilibrium optimizer: A novel optimization algorithm. *Knowledge-Based Systems* **2019**, p. 105190.
36. Biswas, P.P.; Suganthan, P.N.; Mallipeddi, R.; Amaratunga, G.A. Optimal power flow solutions using differential evolution algorithm integrated with effective constraint handling techniques. *Engineering Applications of Artificial Intelligence* **2018**, *68*, 81–100.
37. Shaheen, A.M.; El-Sehiemy, R.A.; Farrag, S.M. Solving multi-objective optimal power flow problem via forced initialised differential evolution algorithm. *IET Generation, Transmission & Distribution* **2016**, *10*, 1634–1647.
38. Panda, A.; Tripathy, M. Security constrained optimal power flow solution of wind-thermal generation system using modified bacteria foraging algorithm. *Energy* **2015**, *93*, 816–827.
39. Shargh, S.; Mohammadi-Ivatloo, B.; Seyedi, H.; Abapour, M.; others. Probabilistic multi-objective optimal power flow considering correlated wind power and load uncertainties. *Renewable Energy* **2016**, *94*, 10–21.
40. Biswas, P.P.; Suganthan, P.N.; Qu, B.Y.; Amaratunga, G.A. Multiobjective economic-environmental power dispatch with stochastic wind-solar-small hydro power. *Energy* **2018**, *150*, 1039–1057.
41. Hu, F.; Hughes, K.J.; Ma, L.; Pourkashanian, M. Combined economic and emission dispatch considering conventional and wind power generating units. *International Transactions on Electrical Energy Systems* **2017**, *27*, e2424.

Preprints (www.preprints.org) | NOT PEER-REVIEWED | Posted: 17 September 2020 doi:10.20944/preprints202009.0373.v1

42. Hu, F.; Hughes, K.J.; Ingham, D.B.; Ma, L.; Pourkashanian, M. Dynamic economic and emission dispatch model considering wind power under Energy Market Reform: A case study. *International Journal of Electrical Power & Energy Systems* **2019**, *110*, 184–196.
43. Mirjalili, S. aMFOMoth-flame optimization algorithm: A novel nature-inspired heuristic paradigm. *Knowledge-Based Systems* **2015**, *89*, 228–249.
44. Mirjalili, S.; Lewis, A.; Sadiq, A.S. Autonomous particles groups for particle swarm optimization. *Arabian Journal for Science and Engineering* **2014**, *39*, 4683–4697.
45. Rao, R.V.; Savsani, V.J.; Vakharia, D. aTLBOTeaching–learning-based optimization: an optimization method for continuous non-linear large scale problems. *Information sciences* **2012**, *183*, 1–15.
46. Taha, I.B.; Elattar, E.E. Optimal reactive power resources sizing for power system operations enhancement based on improved grey wolf optimiser. *IET Generation, Transmission & Distribution* **2018**, *12*, 3421–3434.
47. Alsac, O.; Stott, B. Optimal load flow with steady-state security. *IEEE transactions on power apparatus and systems* **1974**.
48. Zimmerman, R.D.; Murillo-Sánchez, C.E.; Gan, D. MATPOWER: A MATLAB power system simulation package. *Manual, Power Systems Engineering Research Center, Ithaca NY* **1997**, *1*.